Advanced Materials Engineering For Sustainable Manufacturing and Energy Applications

Editor
HASAN KÖTEN

BİDGE

BİDGE Yayınları

Advanced Materials Engineering For Sustainable Manufacturing and Energy Applications

Editör: HASAN KOTEN

ISBN: 978-625-372-909-7

1. Baskı
Sayfa Düzeni: Gözde YÜCEL
Yayınlama Tarihi: 2025-12-25
BİDGE Yayınları

Sertifika No: 71374
Yayın hakları © BİDGE Yayınları
www.bidgeyayinlari.com.tr - bidgeyayinlari@gmail.com
Krc Bilişim Ticaret ve Organizasyon Ltd. Şti.
Güzeltepe Mahallesi Abidin Daver Sokak Sefer Apartmanı No: 7/9 Çankaya / Ankara

Advanced Materials and Manufacturing Technologies in Sustainable Engineering Applications

Preface

Engineering disciplines are currently facing complex global challenges, including increasing energy demand, limited natural resources, environmental concerns, and the need for high-performance and cost-effective solutions. In this context, sustainability has become a central concept in modern engineering practice, and advanced materials together with innovative manufacturing technologies play a critical role in addressing these challenges. Developments in materials science, production processes, and system integration enable the design of engineering solutions that are lighter, more durable, energy-efficient, and environmentally responsible. This book, entitled Advanced Materials and Manufacturing Technologies in Sustainable Engineering Applications, brings together recent and original studies conducted across diverse engineering fields such as materials and metallurgical engineering, automotive engineering, and energy systems. The chapters cover a broad range of topics, including precision casting technologies, surface treatment and coating methods, additive manufacturing, biodegradable and biomaterials, green chemistry approaches, thermal energy storage systems, and modeling and simulation of electric vehicle technologies. Each contribution aims to provide both fundamental theoretical insights and practical perspectives relevant to industrial applications. The primary objective of this book is to serve as a comprehensive reference for academics, graduate students, researchers, and industry professionals working in the field of sustainable engineering. It is expected that this volume will promote interdisciplinary collaboration, support the development of innovative and environmentally conscious technologies, and contribute to the advancement of sustainable engineering practices. The editors would like to express their sincere appreciation to all contributing authors for their valuable efforts and hope that this book will provide meaningful guidance for future research and engineering applications.

Prof. Dr. Hasan KÖTEN
Head of Department
Engineering Faculty
İstanbul Medeniyet Üniversitesi

İÇİNDEKİLER

BÖLÜM 1

CALCULATION OF MASS ATTENUATION COEFFICIENTS, EFFECTIVE ATOMIC NUMBERS, ELECTRON DENSITIES AND EXPOSURE BUILDUP FACTORS OF BISMUTH (III) OXIDE REINFORCED AZ91 COMPOSITES

Kadir GÜNOĞLU [1]
Hatice VAROL ÖZKAVAK [2]

1. Introduction

Ionizing radiation, particularly gamma rays and X-rays, is extensively employed in a wide range of fields, including medical imaging and radiotherapy, nuclear power generation, industrial radiography, and space technologies. Nevertheless, exposure to high-energy photons poses significant risks to both human health and sensitive electronic systems. Consequently, the development of effective radiation shielding materials aimed at mitigating the harmful effects of ionizing radiation has become a critical scientific and engineering challenge (Gökçe et al., 2018; Kavaz et al., 2020).

[1] Doç. Dr., Isparta Uygulamalı Bilimler Üniversitesi, Teknik Bilimler Meslek Yüksekokulu, kadirgnoglu@gmail.com, ORCID: 0000-0002-9008-9162.
[2] Doç. Dr., Isparta Uygulamalı Bilimler Üniversitesi, Teknik Bilimler Meslek Yüksekokulu, hvarol32@gmail.com, ORCID: 0000-0002-0314-0119.

Conventional shielding materials such as lead and concrete exhibit high attenuation capabilities; however, their high densities, toxicity, limited formability, and poor portability impose substantial limitations in modern engineering applications (Dong et al., 2021; Almuqrin et al., 2021; Aygün, 2021).

In this context, growing attention has been directed toward alternative radiation shielding materials that are lightweight, environmentally benign, and mechanically adequate. Metal matrix composites (MMCs) are regarded as promising material systems for such applications due to their tunable physical and mechanical properties, manufacturing versatility, and potential for functional design (Akkurt et al., 2014; Rashed et al., 2021; Rashed et al., 2023). Among them, magnesium and magnesium-based alloys have attracted considerable interest in weight-sensitive applications owing to their extremely low density, high specific strength, and good castability (Daoush et al., 2023; Mohrez, 2025).

The AZ91 magnesium alloy (Mg–Al–Zn) is among the most extensively employed Mg-based alloys due to its favorable combination of mechanical performance, comparatively good corrosion resistance, and broad industrial accessibility (Song et al., 2020; Yang et al., 2020). Nevertheless, the relatively low atomic number (Z) of magnesium inherently limits the photon shielding capability of AZ91, particularly against high-energy radiation. In photon–matter interactions, the attenuation efficiency of a material is primarily governed by parameters such as density, effective atomic number, and elemental composition (Sahoo and Panigrahi, 2019; Dargusch et al., 2020). Depending on the photon energy range, different interaction mechanisms—including the photoelectric effect, Compton scattering, and pair production—become predominant, and these processes are strongly influenced by the incorporation of high-Z constituents (Asgari et al., 2021; Özkan et al., 2023). Consequently, the integration of high-atomic-number

phases into low-density metallic matrices has become a widely adopted approach for designing lightweight materials with improved radiation shielding performance (Reddy et al., 2022).

In recent years, increasing emphasis has been placed on the development of non-toxic heavy-metal-based materials as substitutes for conventional lead shielding. Within this context, bismuth and its compounds have attracted significant interest owing to their high atomic number (Bi, Z = 83), elevated density, and environmentally benign characteristics (Coomaraswamy et al., 2007; Azimkhani et al., 2019). Among these compounds, bismuth(III) oxide (Bi_2O_3) stands out as an effective ceramic reinforcement for gamma- and X-ray attenuation applications due to its high density and enhanced effective atomic number (El-khatib et al., 2021; Elsafi et al., 2021). Numerous studies in the literature have reported that the incorporation of Bi_2O_3 into polymer and metal matrix composites leads to significant increases in mass attenuation (MAC) values while improving other protection degradation (Yılmaz et al., 2020; Asgari et al., 2021; Elsafi et al., 2021).

A review of the existing literature indicates that systematic investigations focusing on the radiation shielding performance of AZ91 alloys reinforced with varying volume fractions of Bi_2O_3 remain limited. In particular, comprehensive assessments of the effects of Bi_2O_3 volume fraction on chemical composition, density variation, and gamma-ray attenuation parameters are still lacking. Such analyses are of critical importance for the design of lightweight, lead-free, and high-performance radiation shielding materials.

In this study, the gamma ray shielding properties of AZ91 matrix composites reinforced with 0%, 5%, 15%, and 30% Bi_2O_3 by volume were theoretically investigated using the Phy-X/PSD database. Results obtained for mass attenuation coefficients (MAC), linear attenuation coefficients (LAC), the effective atomic number

(Z_{eff}), effective electron density (N_{eff}), and exposure buildup factor (EBF) parameters over a wide photon energy range were used to evaluate the effects of Bi_2O_3 reinforcement on the radiation shielding properties of the AZ91 alloy. The evaluation considered variations in photon energy, material ratios within the composite, and atomic number changes.

2. MATERIALS AND METHODS

In this study, magnesium alloy (AZ91) based composites reinforced with different ratios of bismuth(III) oxide (Bi_2O_3) were investigated. AZ91 powder was used as the matrix material at ratios of 0%, 5%, 15%, and 30% Bi_2O_3. The composite samples were coded as AZ91 (unreinforced), AZ91 5% BiO (5% Bi_2O_3), AZ91 15% BiO (15% Bi_2O_3), and AZ91 30% BiO (30% Bi_2O_3).

To assess the radiation shielding characteristics of the investigated samples, a series of attenuation-related parameters were determined over a photon energy range of 0.015–15 MeV using the Phy-X/PSD computational tool. Phy-X/PSD is a comprehensive simulation-based software designed for the analysis of radiation–matter interaction phenomena and the evaluation of shielding efficiency of materials subjected to ionizing radiation.

By employing theoretical photon interaction cross-section databases together with established physical interaction models, Phy-X/PSD accounts for both the chemical composition and density of the material system. This approach enables accurate evaluation of shielding parameters for pure elements, compounds, alloys, and composite materials. Owing to its adaptable input framework and energy-dependent analytical capability, Phy-X/PSD has become a reliable and extensively utilized platform for comparative radiation shielding assessments in fields such as medical physics, nuclear engineering, and radiation protection studies.

In contrast to the interaction mechanisms of charged particles, the interaction of photons with matter exhibits fundamentally different characteristics. When a photon beam penetrates a material, a portion of the photons is absorbed within the medium, some pass through without undergoing any interaction, while others are scattered away from their initial trajectories, particularly at lower photon energies. The probability of these interaction processes is strongly dependent on the incident photon energy, the composition and density of the shielding material, and the prevailing experimental conditions. A higher degree of attenuation for a given material thickness indicates superior shielding effectiveness. Consequently, the selection of an appropriate radiation shielding material is primarily based on the attenuation behavior described by the Beer–Lambert law (Bashter, 1997). This law, also referred to as the exponential attenuation law, quantitatively relates the transmitted gamma-ray intensity to the incident intensity as a function of material thickness.

$$I = I_0 e^{-\mu x} \quad (1)$$

I_0 represents the initial gamma-ray intensity from the radioactive source in this formulation, while I represents the transmitted gamma-ray intensity measured following the installation of the shielding material between the source and the detector. The shielding layer thickness is denoted by x, and LAC is represented by the value μ (cm^{-1}). Normalizing LAC with regard to the material density yields the MAC, which is defined as μ/ρ and represented in cm^2g^{-1} (Gunoglu et al., 2021). The following relation can be used to determine MAC for composite systems at a specific photon energy:

$$\mu_m = (\mu/\rho) = \sum_i w_i \, (\mu/\rho)_i \quad (2)$$

In this case, $(\mu/\rho)_i$ is the MAC of the i_{th} constituent element in the chemical composition of the shielding material, and w_i is the weight fraction (% Wf.).

In order to describe the likelihood of photon-matter interaction at the atomic and electronic levels, two crucial parameters are the total atomic cross section (σ_t) and the total electronic cross section (σ_e). While the σ_e describes the possibility of a contact per electron, the σ_t shows the cumulative probability of photon interactions with an atom, accounting for all potential interaction pathways (Gunoglu et al., 2021). The evaluation of Z_{eff} and N_{eff}, two crucial parameters for describing the radiation attenuation behavior of composite and heterogeneous materials, is based on these cross sections. The Z_{eff} provides a single representative value that reflects the overall atomic response of a material to photon irradiation, while the N_{eff} describes the number of electrons available for photon interactions per unit mass or volume. The values of σ_t, σ_e, Z_{eff}, and N_{eff} are strongly energy-dependent and are calculated using the following equations (Gunoglu et al., 2021; Tekin et al., 2020):

$$\sigma_t = \frac{\mu_m N}{N_A}, \quad \sigma_e = \frac{1}{N_A}\sum_i \frac{f_i N_i}{Z_i}(\mu_m)_i = \frac{\sigma_t}{Z_{eff}} \tag{3}$$

Where

N : Atomic mass of materials $(N = \sum_i n_i A_i)$

N_A : The Avagadro's number

Z_i : The atomic number of i_{th} element

f_i : The fractional abundance of the element

$$Z_{eff} = \frac{\sigma_t}{\sigma_e}, \quad N_e = \frac{N_A}{N} Z_{eff} \sum_i n_i = \frac{\mu_m}{\sigma_e} \tag{4}$$

The determination of the equivalent atomic number (Z_{eq}) and the corresponding geometric progression (GP) fitting parameters is a prerequisite for evaluating the EBF of AZ91 composites incorporating different weight fractions of Bi_2O_3. To calculate the Z_{eq} values of a composite material, both the total mass attenuation

coefficient $(\mu/\rho)_{Total}$ and the Compton scattering partial mass attenuation coefficient $(\mu/\rho)_{Comp}$ must be determined (Singh et al., 2008). The ratio of these coefficients reflects the relative contribution of Compton scattering to the overall photon interaction processes within the material and serves as the basis for defining an effective atomic representation. The Z_{eq} values are then obtained through interpolation using the following equation:

$$Z_{eq} = \frac{Z_1(logR_2 - logR) + Z_2(logR - logR_2)}{logR_2 - logR_1} \quad (5)$$

In addition, the ratio between the Compton scattering $(\mu/\rho)_{Comp}$ and $(\mu/\rho)_{Total}$, commonly referred to as the incoherent scattering–to–total attenuation ratio, can be evaluated using the following expression:

$$R_{inc/total} = \frac{(\mu/\rho)_{Comp}}{(\mu/\rho)_{Total}} \quad (6)$$

Once Z_{eq} values are determined in the initial step, the corresponding geometric progression (G–P) fitting parameters for any shielding material can be obtained using an interpolation procedure identical to that employed in the Z_{eq} calculation (Tekin et al., 2020). This relationship is expressed as:

$$P = \frac{P_1(logZ_2 - logZ_{eq}) + P_2(logZ_{eq} - logZ_1)}{logZ_2 - logZ_1} \quad (7)$$

where P1 and P2 stand for the G–P fitting parameters that, respectively, correspond to the reference atomic numbers Z1 and Z2. The ANSI/ANS-6.4.3 standard reference database (ANSI/ANS-6.4.3, 1991) provided the G–P fitting parameters used in this investigation.

The G–P fitting parameters calculated using the above expressions are subsequently employed to estimate the EBF values for shielding materials (Singh et al., 2008). The EBF as a function of photon energy E and penetration depth X is given by:

$$B(E,X) = 1 + \frac{b-1}{K-1}.(K^x - 1) \quad \text{for } K \neq 1 \qquad (8)$$

$$B(E,X) = 1 + (b-1).x \quad \text{for} K = 1 \qquad (9)$$

The parameter K(E,X) is defined as:

$$K(E,X) = cx^a + d.\frac{tanh\left(\frac{x}{X_k}-2\right)-tanh(-2)}{1-tanh(-2)} \quad \text{for } x \leq 40MFP \ (10)$$

X signifies the penetration depth expressed in relation to the mean free path (MFP), whereas E defines the energy of the incident gamma rays. The parameters b, c, a, d, and Xk are the G–P fitting coefficients that define the material-specific accumulation behavior.

3. RESULTS AND DISCUSSION

The dependence of the MAC (Figure 1) and LAC (Figure 2) on photon energy for the AZ91 alloy and its composites reinforced with 5%, 15%, and 30% Bi_2O_3 demonstrates systematic and physically meaningful behavior when photon–matter interaction mechanisms are evaluated in conjunction with composite composition. A detailed assessment of the corresponding curves indicates that both MAC and LAC values are strongly influenced by photon energy as well as by the Bi_2O_3 content of the material.

Figure 1. MAC values for the AZ91– Bi_2O_3 composites

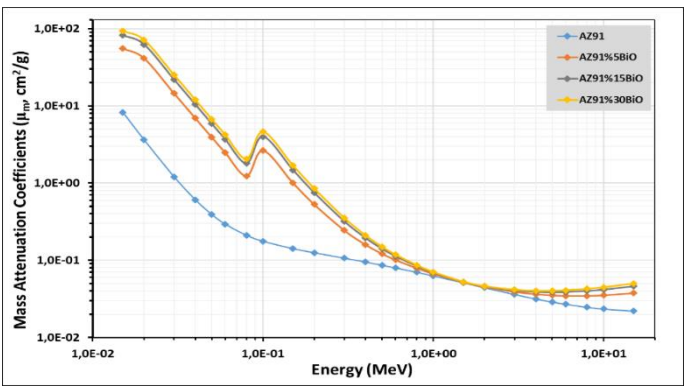

Figure 2. LAC values for the AZ91– Bi_2O_3 composites

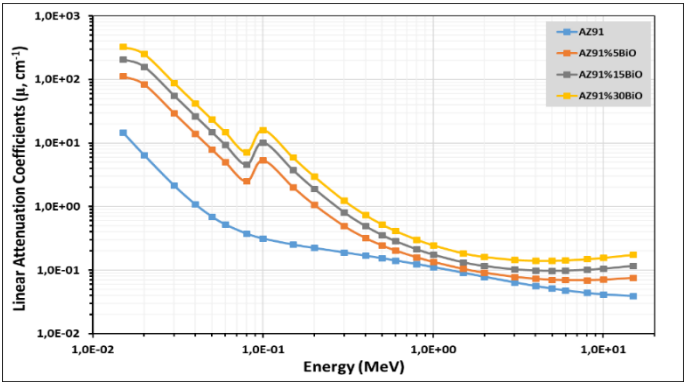

At low photon energies (≈0.01–0.05 MeV), all samples exhibit high MAC and LAC values followed by a sharp decrease with increasing energy, reflecting the dominance of the photoelectric absorption mechanism. Due to the strong atomic number dependence of this interaction, Bi_2O_3-reinforced composites—particularly those containing 15% and 30% Bi_2O_3—show significantly higher attenuation coefficients than the unreinforced AZ91 alloy, which consists mainly of low-Z elements. Minor oscillations and localized peaks observed in the low-energy MAC and LAC curves of Bi_2O_3-containing composites are attributed to the L and K absorption edges of bismuth. In the intermediate energy range (≈0.05–1 MeV), Compton scattering becomes the predominant interaction mechanism, leading to a more gradual decrease and convergence of the attenuation curves, as this process depends weakly on atomic number. Nevertheless, the increased electron density provided by Bi_2O_3 addition allows the reinforced composites to maintain higher MAC and LAC values than AZ91. At higher photon energies (≳1 MeV), the attenuation coefficients approach minimum values, and the onset of pair production results in a slight increase or plateau behavior for composites with higher Bi_2O_3 content, with the 30% Bi_2O_3 sample exhibiting the highest attenuation performance in this region, while the AZ91 alloy shows

only a marginal enhancement due to its lower effective atomic number.

The energy-dependent variation of the Z_{eff} values for AZ91 alloy and composites produced with Bi_2O_3 addition is shown in Figure 3.

Figure 3. Z_{eff} values for the AZ91– Bi_2O_3 composites

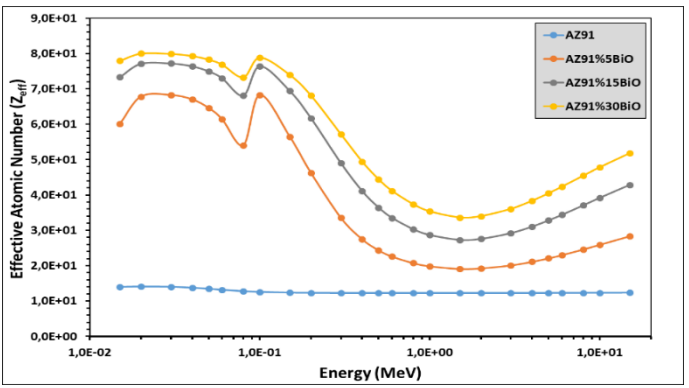

In the low-energy region (≈0.01–0.05 MeV), the Z_{eff} values of Bi_2O_3-reinforced composites are significantly higher than those of the unmodified AZ91 alloy and increase with increasing Bi_2O_3 content. While AZ91 exhibits low and nearly energy-independent Z_{eff} values, composites containing 15% and 30% Bi_2O_3 reach maximum Z_{eff} levels due to the dominance of photoelectric absorption and the strong atomic number dependence of this interaction ($\propto Z^4$–Z^5), highlighting the critical role of high-Z bismuth. As photon energy increases into the intermediate range (≈0.05–1 MeV), Z_{eff} values decrease markedly for all samples and the curves converge, reflecting the predominance of Compton scattering, which depends weakly on atomic number and is governed primarily by electron density. Although Bi_2O_3-containing composites retain higher Z_{eff} values than AZ91, the separation among samples is substantially reduced in this region. At higher energies (≳1 MeV), Z_{eff} exhibits a renewed increasing trend due to

the onset of pair production, whose cross-section scales approximately with Z^2, resulting in a more pronounced enhancement for composites with higher Bi_2O_3 content, particularly the 30% Bi_2O_3-reinforced sample.

The energy-dependent variation of N_{eff} values for AZ91 alloy and composites produced with Bi_2O_3 addition is shown in Figure 4.

Figure 4. Z_{eff} values for the AZ91– Bi_2O_3 composites

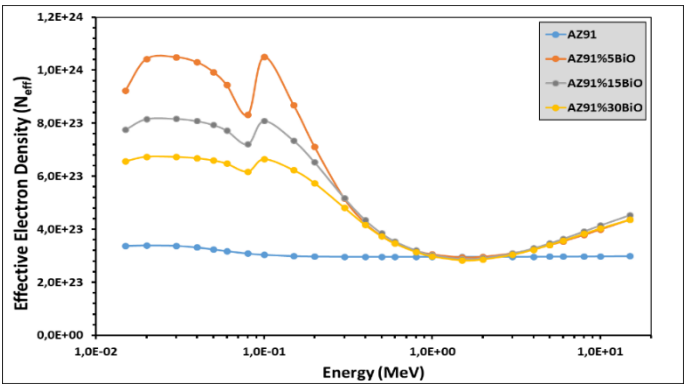

An examination of the N_{eff} values indicates that, although their energy-dependent variation follows a trend similar to that of Z_{eff}, they represent a distinct physical interpretation. In the low-energy region, the Neff values of Bi_2O_3-reinforced composites are significantly higher than those of the pure AZ91 alloy due to the increased total electron number and electron density introduced by Bi_2O_3 addition. Notably, even the composite containing 5% Bi_2O_3 exhibits a pronounced increase in N_{eff}, indicating that small amounts of high-Z filler can substantially enhance electron density and, consequently, photoelectric interaction probability. As photon energy increases into the intermediate region, N_{eff} values decrease and then approach a nearly constant plateau, reflecting the dominance of Compton scattering, where attenuation is governed primarily by electron density rather than atomic number. In this regime, differences in N_{eff} among composites with varying Bi_2O_3

contents become less distinct, while the relatively stable N_{eff} values of the AZ91 alloy are characteristic of a low-Z, homogeneous matrix under Compton-dominated conditions. At higher photon energies, N_{eff} exhibits a renewed increase due to electron–positron pair production and subsequent secondary interactions. This effect becomes more pronounced with increasing Bi_2O_3 content, with the 15% and 30% Bi_2O_3-reinforced composites showing markedly higher N_{eff} values than the unreinforced AZ91 alloy, underscoring the effectiveness of heavy-element reinforcement in high-energy gamma-ray shielding.

The energy-, composition-, and mean free path (MFP)-dependent variation of the exposure buildup factor (EBF) for AZ91 alloy and Bi_2O_3-reinforced composites is presented in Figures 5–8. Since the EBF accounts for the cumulative contribution of scattered photons and secondary radiation reaching the detector, its magnitude is strongly influenced by photon interaction mechanisms, atomic number effects, and geometrical factors such as material thickness. Consequently, pronounced increases in EBF values are observed in energy regions where high-Z contributions and multiple scattering processes become significant.

Figure 5. EBF values for the AZ91

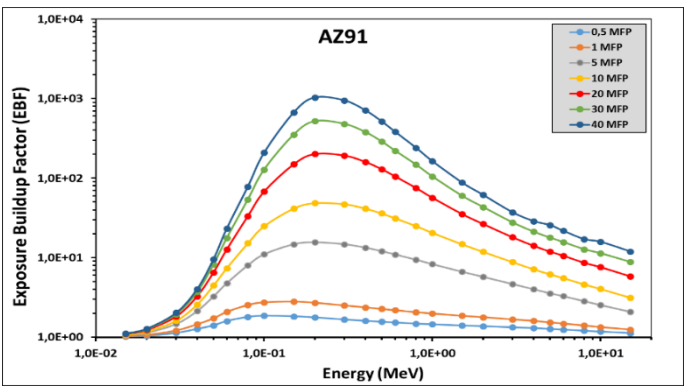

Figure 6. EBF values for the AZ91%5Bi_2O_3 composite

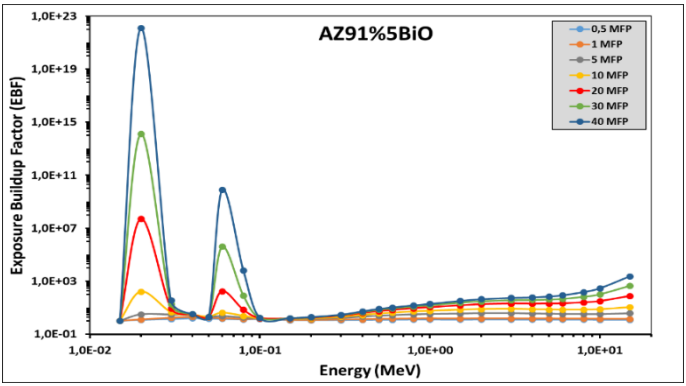

Figure 7. EBF values for the AZ91%15Bi_2O_3 composite

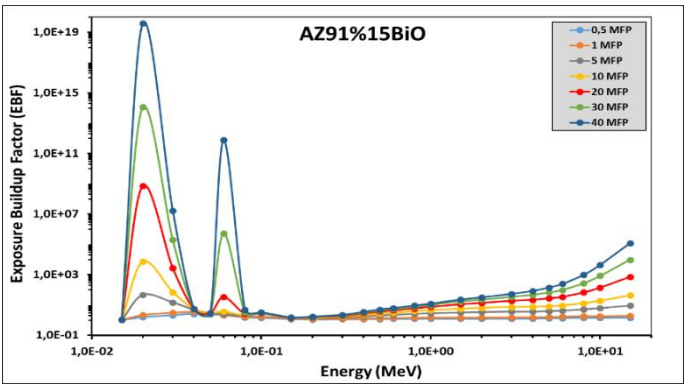

Figure 8. EBF values for the AZ91%30Bi_2O_3 composite

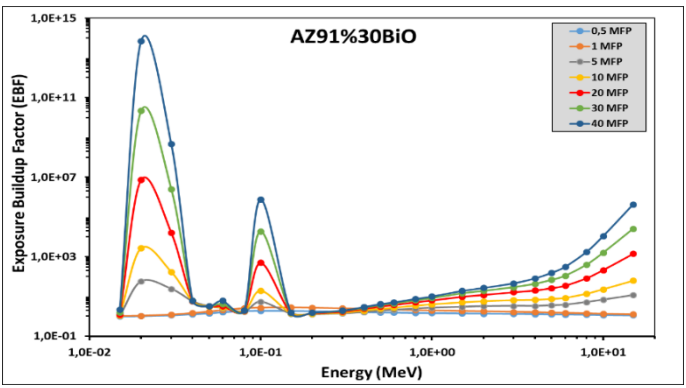

In the low-energy region (≈0.01–0.05 MeV), all samples exhibit a sharp increase in EBF values due to the dominance of photoelectric absorption, which strongly depends on atomic number. The pure AZ91 alloy, composed mainly of low-Z elements (Mg, Al, and Zn), shows relatively low and nearly uniform EBF maxima, whereas Bi_2O_3 incorporation markedly enhances the effective atomic number and the probability of photoelectric interactions. The presence of sharp and intense EBF peaks at low energies—even for the composite containing 5% Bi_2O_3—is attributed to photon interactions near the characteristic absorption edges of bismuth. For composites with 15% and 30% Bi_2O_3, these peaks increase by several orders of magnitude, indicating pronounced photon buildup caused by enhanced scattering and secondary photon generation.

In the intermediate energy range (≈0.05–1 MeV), EBF values decrease significantly and exhibit a plateau-like behavior for all samples, reflecting the predominance of Compton scattering. Owing to the weak atomic number dependence of this mechanism, variations in Bi_2O_3 content have a limited effect, leading to convergence of the EBF curves and indicating reduced photon accumulation within the material.

At higher photon energies (≳1 MeV), EBF values increase again with the onset of pair production. Because the pair production cross-section scales approximately with Z^2, composites with higher Bi_2O_3 content—particularly those containing 15% and 30% Bi_2O_3—show a pronounced, near-logarithmic rise in EBF, signifying sustained photon buildup through secondary radiation processes. In contrast, the pure AZ91 alloy exhibits only a modest increase due to its lower effective atomic number. From the perspective of the mean free path parameter, EBF values are found to increase substantially with increasing MFP for all composites. A larger MFP corresponds to longer photon travel distances within the material, thereby increasing the likelihood of repeated scattering and secondary

interaction events. While EBF values remain relatively low at small penetration depths (0.5–1 MFP), they rise dramatically at larger depths, such as 20–40 MFP, particularly in composites with high Bi_2O_3 content. This behavior clearly highlights the critical influence of material thickness and geometrical configuration on photon buildup phenomena.

4. CONCLUSION

The gamma radiation shielding performance of AZ91 alloy and AZ91– Bi_2O_3 composites was systematically evaluated using the Phy-X/PSD software over a wide photon energy range. The results indicate that increasing the Bi_2O_3 content leads to a clear enhancement in the attenuation-related parameters, including MAC, LAC, Z_{eff}, and N_{eff}, particularly in the low-energy region where the photoelectric effect dominates. This improvement is directly associated with the high atomic number and density of bismuth.

In the intermediate energy range, where Compton scattering is the prevailing interaction mechanism, the variation in shielding parameters with composition becomes less pronounced, and the values tend to converge. At higher photon energies, a moderate but consistent increase in attenuation performance is observed for Bi_2O_3-rich composites due to the contribution of pair production processes.

The buildup factor analysis shows that both EBF and EABF increase with Bi_2O_3 content and mean free path, with EBF systematically exceeding EABF as a result of scattered and secondary photon contributions. These findings quantitatively demonstrate that although higher Bi_2O_3 contents improve attenuation efficiency, they also intensify buildup effects, especially at large thicknesses. Overall, AZ91– Bi_2O_3 composites can be considered promising lightweight shielding materials, provided that the Bi_2O_3ratio and shielding geometry are optimized according to the operating photon energy range.

REFERENCES

Akkurt, I., Günoğlu, K., Çalik, A., & Karakas, M., (2014). Determination of gamma ray attenuation coefficients of Al-4% Cu/B 4 C metal matrix composites at 662, 1173 and 1332 keV. Bulletin of Materials Science 37, 1175-1179

Almuqrin, A.H., Sayyed, M.I., (2021). Radiation shielding characterizations and investigation of TeO2– WO3–Bi2O3 and TeO2–WO3–PbO glasses. Appl. Phys. A 127 (3), 1–11.

ANSI/ANS-6.4.3, Gamma ray attenuation coefficient and buildup factors for engineering materials, American Nuclear Society, La Grange Park, Illinois (1991)

Asgari, M., Afarideh, H., Ghafoorifard, H., Amirabadi, E.A., (2021). Comparison of nano/ micro lead, bismuth and tungsten on the gamma shielding properties of the flexible composites against photon in wide energy range (40 keV-662 keV), Nucl. Eng. Technol. 53, 4142-4149.

Aygün, B., 2021. Neutron and gamma radiation shielding Ni based new type super alloys development and production by Monte Carlo Simulation technique. Radiat. Phys. Chem. 188, 109630

Azimkhani, S., Kalhor, A., Rahmani, A., Sohrabi, A., (2019). Investigation of gamma-ray shielding and strength properties of concrete containing bismuth and barite. Iran. J. Sci. Technol. Trans. A-Science 43 (4), 1967–1972.

Bashter, I.I., (1997). Calculation of radiation attenuation coefficients for shielding concretes. Ann. Nucl. Energy 24, 1389.

Coomaraswamy, K.S., Lumley, P.J., Hofmann, M.P., (2007). Effect of bismuth oxide radioopacifier content on the material properties of an endodontic Portland cement–based (MTA-like) system. J. Endod. 33 (3), 295–298.

Daoush, W. M., El-Tantawy, A., Morsi, K., El-Nikhaily, A. E., (2023). Novel Cubic Boron Nitride-Reinforced Cu/Ni Alloy Elemental Metal Matrix Composites for Electromagnetic Radiation Shielding Applications. Journal of Materials Engineering and Performance, 1-13

Dargusch, M.S., Balasubramani, N., Venezuela, J., Johnstona, S., Wang, G., Lau, C., Bermingham, M., Kentc, D., StJohn, D.H., (2020). Improved biodegradable magnesium alloys through advanced solidification processing, Scr. Mater. 177, 234–240,

Dong, M., Zhou, S., Xue, X., Feng, X., Sayyed, M.I., Khandaker, M.U., Bradley, D.A., (2021). The potential use of boron containing resources for protection against nuclear radiation. Radiat. Phys. Chem. 188, 109601.

El-khatib, A.M., Elsafi, M., Sayyed, M.I., Abbas, M.I., El-Khatib, M., (2021). Impact of micro and nano aluminium on the efficiency of photon detectors. Results Phys. 30, 104908.

Elsafi, M., Sayyed, M.I., Almuqrin, A.H., Gouda, M.M., El-Khatib, A.M., (2021). Analysis of particle size on mass dependent attenuation capability of bulk and nanoparticle PbO radiation shields. Results Phys. 26, 104458

Gökçe, H.S., Öztürk, B.C., Çam, N.F., Andiç-Çakır, Ö., (2018). Gamma-ray attenuation coefficients and transmission thickness of high consistency heavyweight concrete containing mineral admixture. Cement Concr. Compos. 92, 56–69.

Kavaz, E., Ghanim, E.H., Abouhaswa, A.S., (2020). Optical, structural and nuclear radiation security properties of newly fabricated V2O5-SrO-PbO glass system. J. Non-Cryst. Solids 538, 120045.

Mohrez, W. A., (2025). High performance Aluminum matrix composite for radiation shielding. Egypt. J. Chem. Vol. 68, pp. 509 - 521

Özkan, Z., Gökmen, U., Ocak, S.B., (2023). Analyses of Gamma and Neutron Attenuation Properties of the AA6082 composite material doped with boron carbide (B4C), 110810, Radiat. Phys. Chem. 206

Rashed, G. M., Sadawy, M. M., Kandil, A. A., Abdelkareem, A., Mohrez, W. A., (2023). Corrosion Behavior of AlMg5/10ZrO2 Metal Matrix Composite in 3.5 wt% NaCl Solution. Journal of Bio-and Tribo-Corrosion 9, 36

Rashed, G., Sadawy, M., Kandil, A., Abd Elkarim, A., Mohrez, W., (2021). Influence of ZrO2 particles on the tribological properties of AlMg5 alloy. Journal of Petroleum and Mining Engineering, vol. 23, no. 1, pp. 95-103.

Reddy, B.C., Manjunatha, H.C., Vidya, Y.S., Sridhar, K.N., Pasha, U.M., Seenappa, L., Sadashivamurthy, B., Dhananjaya, N., Sathish, K.V., Gupta, P.S.D., (2022). X-ray/gamma ray radiation shielding properties of α-Bi2O3 synthesized by low temperature solution combustion method, Nucl. Eng. Technol. 54 (3), 1062–1070.

Sahoo, B.N., Panigrahi, S.K., (2019). Deformation behavior and processing map development of AZ91 Mg alloy with and without addition of hybrid in-situ TiC+TiB2 reinforcement, J. Alloy. Compd. 776, 865–882,

Singh, PS., Singh, T., Kaur P., (2008). Variation of energy absorption buildup factors with incident photon energy and penetration depth for some commonly used solvents. Ann Nucl Energy, 35-6, 1093-1097.

Song, J.F., She, J., Chen, D.L., Pan, F.S., (2020). Latest research advances on magnesium and magnesium alloys worldwide, J. Magnes. Alloy. 8, 1–41,

Şakar, E., Özpolat, Ö.F., Alım, B., Sayyed, M.I., Kurudirek, M., (2020). Phy-X/PSD: development of a user friendly online software for calculation of parameters relevant to radiation shielding and dosimetry, Radiat. Phys. Chem. 166, 108496

Tekin, H.O., Abouhaswa, A.S., Kilicoglu, O., Issa, S.A.M., Akkurt, I., Rammah, Y.S., (2020). Fabrication, physical characteristic, and gamma-photon attenuation parameters of newly developed molybdenum reinforced bismuth borate glasses, Phys. Scr. 95, 115703.

Yang, Y., Xiong, X.M., Chen, J., Peng, X.D., Chen, D.L., Pan, F.S., (2021). Research advances in magnesium and magnesium alloys worldwide in 2020, J. Magnes. Alloy. 9, 705–747.

Yılmaz, S.N., Güngör, A., Özdemir, T., (2020). The investigations of mechanical, thermal and rheological properties of polydimethylsiloxane/bismuth (III) oxide composite for X/Gamma ray shielding. Radiat. Phys. Chem. 170, 108649.

BÖLÜM 2

INVESTIGATION OF THE EFFECT OF GLASS BEAD BLASTING SURFACE TREATMENT ON THE BORIDING KINETICS AND MECHANICAL PROPERTIES OF ADDITIVELY MANUFACTURED MS1 (AISI 18Ni M300) MARAGING STEEL

1. Şirkan Erten KANATOĞLU[1]
2. Erdem ÖZKAN[2]
3. Begüm ERBAŞ[3]
4. Fuat ÇAKIR[4]
5. Özgür ÇINAR[5]
6. Mehmet Masum TÜNÇAY[6]

[1] Marmara University Faculty of Engineering, Metallurgical and Materials Engineering, Orcid: 0009-0002-3608-1415
[2] Marmara University Faculty of Engineering, Metallurgical and Materials Engineering, Orcid: 0009-0008-7757-6370
[3] Marmara University Faculty of Engineering, Metallurgical and Materials Engineering, Orcid: 0009-0000-2912-2851
[4] Marmara University Faculty of Engineering, Metallurgical and Materials Engineering, Orcid: 0009-0006-9065-8990
[5]Res.Asst., Marmara University Faculty of Engineering, Metallurgical and Materials Engineering, Orcid: 0000-0001-6787-4229

INTRODUCTION

Steels are widely used in industrial applications due to their high mechanical strength, hardness, and wear resistance. These properties can be optimized through alloying with carbon and other alloying elements, as well as through heat treatment. Among steels, maraging steels are notable for their combination of low carbon content and high nickel composition, which provides exceptional strength and toughness. This makes them particularly suitable for high-performance applications such as aerospace, automotive, and tooling industries (Behl et al., 2025).

The surface properties of maraging steels, such as hardness and wear resistance, directly influence their service life and performance. In some cases, surface enhancement techniques, including thermal and chemical treatments, are applied to improve these properties. For example, plasma nitriding can significantly increase the surface hardness and wear resistance of maraging steels (Godec et al., 2021).

Additive Manufacturing is an innovative production technology that enables the fabrication of parts with complex geometries with high precision while minimizing material waste. Especially for the production of materials with high corrosion resistance, such as MS1 maraging steel, additive manufacturing methods offer several advantages over conventional manufacturing techniques. However, the microstructural properties and surface qualities of materials produced by additive manufacturing can vary depending on the post-processing procedures applied (Turk et al., 2019).

The boriding process is a widely used thermo-chemical surface hardening method aimed at increasing the surface hardness

[6]Assoc.Prof., Marmara University Faculty of Engineering, Metallurgical and Materials Engineering, Orcid: 0000-0002-1624-5454

and wear resistance of materials. In this process, boron atoms diffuse into the material's surface, forming a hard and durable layer. On the other hand, the glass bead blasting surface treatment is significant in terms of controlling surface roughness and providing improvements in mechanical properties (Kayali & Mertgenç, 2020).

In this study, the boriding kinetics of additively manufactured MS1 maraging stainless steel were examined in detail, and the effects of glass bead blasting surface treatment on the boriding behaviour and mechanical properties were evaluated. The results obtained aim to shed light on the potential of advanced surface treatments to enhance the performance of additively manufactured materials. In the last step, all the data will be analyzed to evaluate the efficiency of the boriding process.

MATERIALS AND METHODS

The study was a five-stage process, starting from sample preparation to the evaluation of results. The manufacturing and surface treatment techniques were applied to the samples in the first stage, while the second stage performed the boriding process, determining the surface preparation and process parameters. The third phase involved mechanical testing and microstructure observation of the boride layers. The fourth phase included data gathering and computation of activation energy. In the last phase, the results were analyzed to assess the efficiency of the boriding treatment and reported. These work packages are prepared to ensure the regular and fruitful progress of each phase of the research.

Sample Preparation Phase

The first work package addresses the production and preparation processes for the samples used in the research. The designs of the samples were drawn using a CAD program, and the

STL files were sent to the manufacturing device. The samples were produced using the Direct Metal Laser Sintering (DMLS) method with the EOS M290 device. The materials used include maraging MS1 steel. A total of 22 samples, each measuring 9x9x3 mm (0.243 cm^3), grouped with nine main samples and two spares per group. Half of the samples undergo sandblasting surface treatment by glass bead blasting with glass beads of 70-110 μm particle size. Once each prefabricated, untreated steel sample was sampled, three XRF analyses were performed on each sample. For each resulting elemental percentage, the average was calculated, and the data were listed. Additionally, the average surface roughness of as-built and glass bead-blasted samples was measured using a Mitutoyo SJ-500 surface roughness measuring system. The measurements were taken on horizontal surfaces (9x9 mm) that were perpendicular to the building direction.

Process Phase

In the actual work package, production and preparation procedures were carried out for the samples to be used in the research. The samples were designed with the aid of a design program and, after that, were sent as STL files to the manufacturing device. These fabricated via the DMLS method with the help of the EOS M290 apparatus. The materials used are maraging MS1 steel. Samples, 22 in total, measuring 9x9x3 mm each, amount to 0.243 cm^3. Group them into nine main samples and two spares per group. Half of the samples undergo surface treatment by glass bead blasting with glass beads of 70-110 μm.

Experiment and Testing Phase

The samples were first cleaned using conventional methods (liquid soap, water, etc.), followed by ultrasonic cleaning with alcohol. The samples were then placed, one by one, in a ceramic

crucible each day with a sufficient amount of Ekabor-II powder. Additionally, SiC powder was placed on the top to provide the optimal thermal insulation. Also, the ceramic crucible, including the sample and boriding powder, was placed in a box made from 310-type steel welded together. After closing the steel box cover, high-temperature sealing paste was applied to the cover's corners. The samples were then borided in a Protherm Box Furnace under pre-determined time and temperature conditions in an air atmosphere.

Metallographic Processes

Metallographic procedures and microscopic examination were conducted on MS1 Maraging Steel specimens in this study. The metallographic procedures carried out are cutting, mounting, grinding, polishing, etching, and microscopic examination (Lawley & Murphy, 2003).

Cutting

After taking out and registering the borided samples, they were cut using a Struers Secotom machine with a 200 mm diameter 50A20 (> HV 500, aluminum oxide) cutting-off wheel. Cutting was performed at low speeds with cutting oil to avoid damaging the boride layers on the samples. This helped to minimize microstructural distortions.

Mounting

For the hot mounting process, a thermosetting resin, bakelite (phenol-formaldehyde based), was used. The samples were placed in the mounting machine, the resin was poured in, and the setup was subjected to specific temperature and pressure conditions (250–350 bar) for 13 minutes for curing.

Mounting preserved the sample edges during grinding and polishing, provided a smoother surface, and allowed clear positioning for microscopic analysis.

Grinding

For MS1 Maraging Steel, silicon carbide (SiC) grinding papers of P180 and P320 grits were used. Since the primary objective was to determine the boride layer thickness, P320 proved to be sufficient in most cases. Polishing and etching after P320 grinding opened the boride layer without wasting time. In certain detailed or sensitive scenarios, grinding was continued up to P1000 grit. All grinding operations were performed with water cooling to prevent surface overheating.

Polishing

One-stage polishing was performed using a particle (1μm) of aluminum oxide suspension. This reduced plastic deformation that could obscure the microstructure and created an optimum surface for microscopic observation.

Etching

MS1 Maraging Steel samples, Aqua Regia was used to reveal the microstructure. Aqua Regia is a mixture of nitric acid and hydrochloric acid in the proportion 3:1. 60 ml hydrochloric acid and 20 ml nitric acid were used (Vander Voort et al., 2004)

To protect individuals from the toxic gases that are emitted during the procedure was carried out under a fume hood.

Etching time was strictly controlled according to the reagent and chemical composition of the material. Over-etching can lead to excessive dissolution and mixing of phases, and therefore, visual observation was crucial (Vander Voort et al., 2004). Through trial and error, it was established that the optimum etching time was approximately 60 seconds for both steels. The samples were washed with alcohol after etching and dried for microscopic examination.

Microscopic Examination

MS1 Maraging Steel samples were conducted using an optical microscope (Nikon) and SEM (ZEISS EVO MA10). The primary motive was to observe the boride layer thicknesses achieved after metallographic preparation.

The microstructures of the samples were imaged at 10X magnification using an optical lens. MS1 samples exhibited well-defined boride layers. The layers were of varying depths depending on the alloying elements and processing conditions of the steel samples. The thicknesses of the boride layers were determined after imaging using ImageJ.

During this stage, various analyses and tests were conducted on the samples after the boriding process. The samples were cut using a diamond saw for delicate work. Cross-sections subjected to metallographic processes and etched with 2% nital (Yapar, 2003; Motallebzadeh et al., 2015). SEM imaging after boriding was carried out by using external service providers. The mechanical tests consisted of microhardness by the Vickers test and surface hardness. Hardness tests made with a 50-gram load using the microhardness Vickers method. These data used to assess the performance of the boriding process (Ozdemir et al., 2008).

Data Collection and Activation Energy Calculations

This is where data acquired in the boriding stage is analyzed. Three corners of every sample where the boride layer was evenly distributed were imaged while measuring the thickness using an optical microscope at a 10X magnification. The images were then processed by utilizing the ImageJ software. For each borided sample, images were taken from three different edges of the sample. Six thickness measurements were taken from each image. The overall average of the 18 measurements per sample was calculated, and this average boride layer thickness was reported as the final result. The

measurement of boride layer thickness and the comparison of hardness values, together with the calculation of the diffusion coefficient using the Arrhenius equation $D = D_0 \times e^{-\frac{Q}{RT}}$ and its correlation with the layer thickness via the relation $x^2 = Dt$ enables the determination of the activation energy, thereby allowing a quantitative characterization of the boriding rate and efficiency. Thickness measurements are planned to be carried out using the ImageJ application. A total of 2 different activation energies are calculated. Separate results obtained for each condition: sandblasted, non-sandblasted, maraging steel, and then a review of the kinetics of the boriding process was also done.

Arrhenius equation and Fick's Law as follows (Kayali & Mertgenç, 2020):

$$D = D_0 \times e^{-\frac{Q}{RT}} \qquad \boldsymbol{Eq.(1)}$$

D_0 = Diffusion constant (cm^2/sec)

Q = Activation energy (J/mol)

T = Temperature (K)

R = Gas constant (8.314 J/mol K)

$$x^2 = D \times t \qquad \boldsymbol{Eq.(2)}$$

x = Boride layer (cm)

D = Diffusion coefficient (cm^2/sec)

t = Boriding time (sec)

$$\ln D = \ln D_0 - \frac{Q}{RT} \qquad \boldsymbol{Eq.(3)}$$

D_0 = Diffusion constant (cm^2/sec)

Q = Activation energy (J/mol)

T = Temperature (K)

R = Gas constant (8.314 J/mol K)

RESULTS AND DISCUSSION

Sample Procurement

This study focused on the thicknesses and mechanical properties of boride layers formed on additively manufactured MS1 maraging steel under different surface conditions and boriding parameters. For samples, elemental composition was evaluated, and the average of XRF analysis results of the samples was presented in Table 1. The average surface roughness of the as-built and glass bead-blasted samples was 3.2 ± 0.4 μm and 3.4 ± 0.4 μm, respectively. Those results were in agreement with some studies in the literature (Vishwakarma et al., 2020; Morel et al., 2018).

Table 1. *XRF results of maraging steel samples*

Maraging XRF Composition	
Element	**Percentage**
Fe	**65.35%**
Ni	**17.70%**
Co	**9.31%**
Mo	**5.19%**
Ti	**1.85%**
Si	**0.27%**
Cr	**0.09%**
Nb	**0.09%**

Thickness and Microhardness of Boriding Layer

The increase in the values of hardness also depended on the parameters of boriding. Figures 1 and 2 are microhardness graphs from the surface to the center of bead-blasted and non-bead-blasted maraging steel samples that were borided at 850 ℃ for 6 hours.

A maximum hardness value was realized at the outer surface in all the samples, which declined sharply while reaching the substrate (matrix) region. Measured microhardness values of borided at 850 ℃ for 6 hours samples were as follows:

- Non-bead-blasted Maraging Steel: 1897 $HV_{0.05}$
- Bead-blasted Maraging Steel: 1857 $HV_{0.05}$

The above findings confirm the effectiveness of the boriding process in enhancing surface hardness, particularly in maraging steel samples.

Figure 1. Microhardness values as a function of distance from the surface for non-bead blasted maraging steel borided at 850°C for 6 hours.

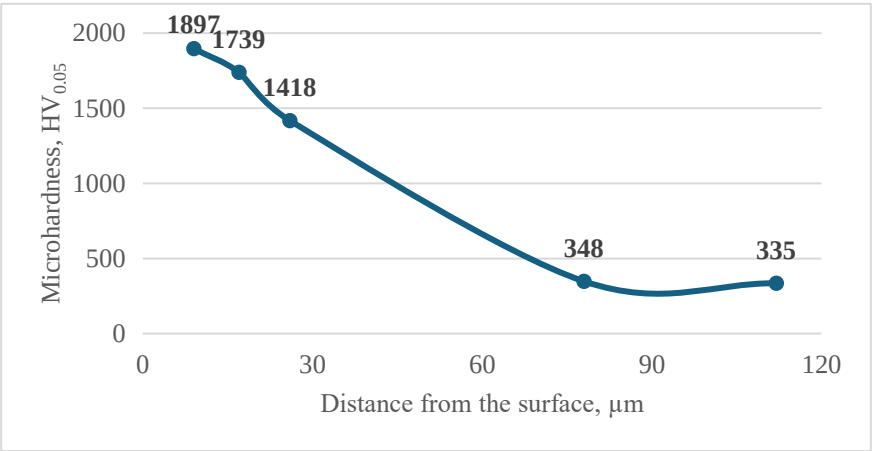

Figure 2. Microhardness values as a function of distance from the surface for bead blasted maraging steel borided at 850°C for 6 hours.

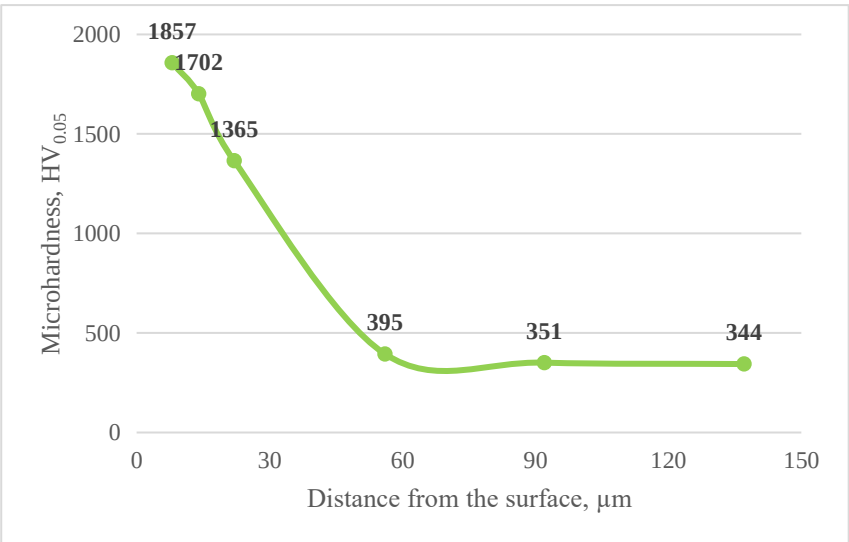

The average thickness of the boride layer formed on bead-blasted and non-bead-blasted samples of maraging steel is revealed through Figures 3 and 4.

Maraging steel samples had comparatively thicker boride layers under identical boriding conditions. Maraging steel samples indicated boride layer thickness ranging from 21.97 µm to 109.36 µm.

Figure 5 shows the effect of alloying elements in steel on boride layer thickness (Dossett & Totten, 2013). Figures 6 Figure **7** show the images acquired at 20X magnification after the microhardness tests. Measurements were taken using a load of 50 grams ($HV_{0.05}$) and a dwell time of 15 seconds. Also, from Figures 8 and 9, SEM images of bead-blasted and non-bead-blasted maraging steel samples can be seen.

Figure 3. Average boride layer thickness of non-bead blasted maraging steel.

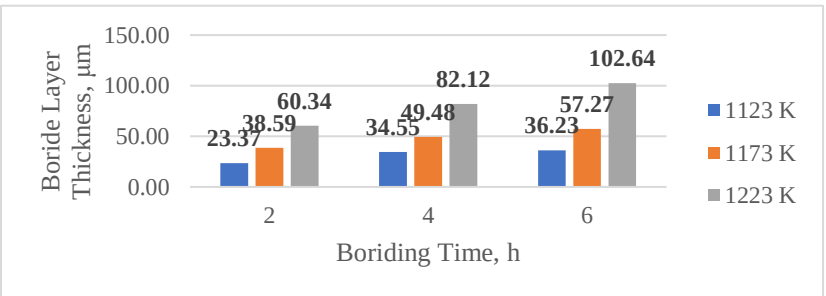

Figure 4. Average boride layer thickness of bead blasted maraging steel.

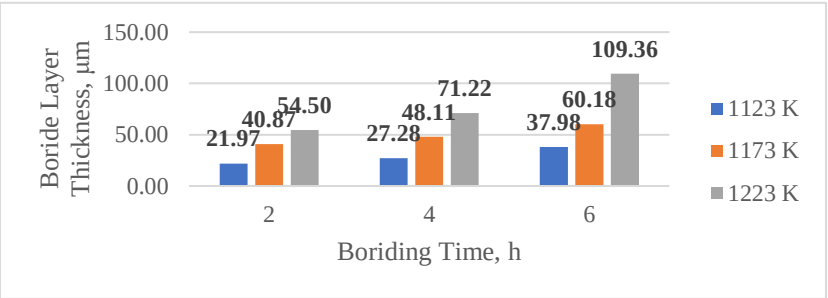

Figure 5. Effect of alloying elements in steel on boride layer thickness. (Dossett & Totten, 2013)

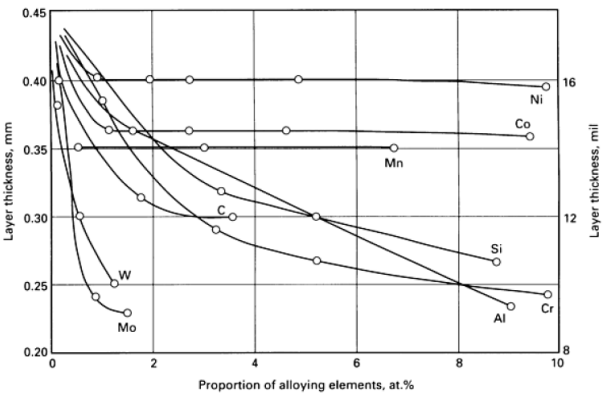

Figure 6. 20X microhardness test image for non-bead blasted maraging steel borided at 850°C for 6 hours.

Figure 7. 20X microhardness image for bead blasted maraging steel borided at 850°C for 6 hours.

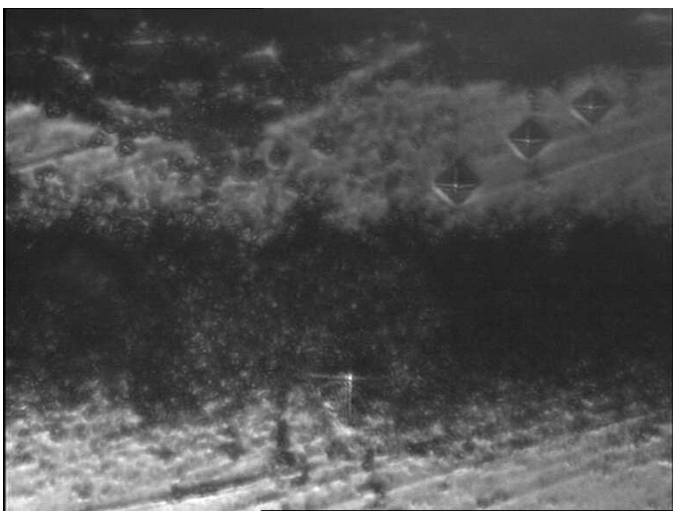

Figure 8. SEM image of non-beadblasted maraging steel borided at 950 °C for 4 hours.

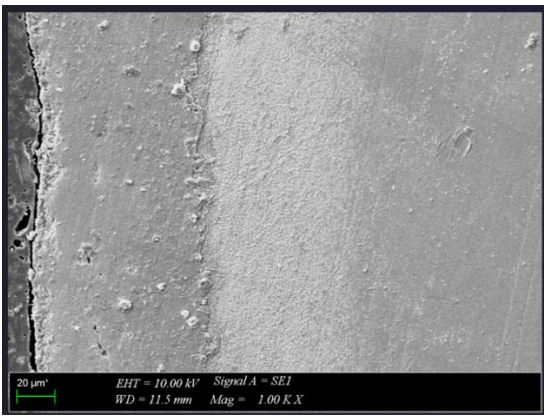

Figure 9. SEM image of beadblasted maraging steel borided at 950 °C for 4 hours.

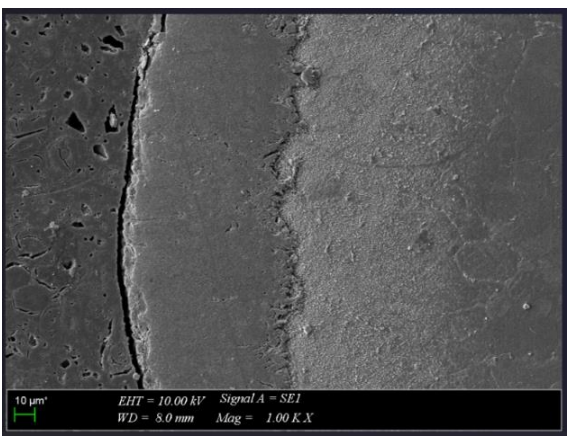

Kinetic

Thicker boride layers were obtained at higher temperatures, due to the increased atomic diffusion rates at higher thermal energies.

Boriding time versus square of boride layer thickness graphs can be observed with Figures 10 and 12. Activation energy (Q) for boron diffusion was calculated from Equation (1) based on the slope of the plot of ln D (logarithm of diffusion coefficient) vs. 1/T (inverse of temperature). The graphs of ln D vs. 1/T for maraging steels (bead blasted and non-blasted) are also presented in Figures 11 and 13.

Activation energy values were determined from these plots as follows:

- Non-blasted maraging steel: 217 kJ/mol

- Bead-blasted maraging steel: 222.97 kJ/mol

The variations in activation energy values observed in boriding processes are primarily governed by several interrelated factors, including the surface condition of the substrate, alloying element content, and processing parameters (Morel et al., 2018; Kayalı & Kara, 2021). Surface treatments can significantly influence boron diffusion by modifying surface roughness and defect density, thereby either impeding or enhancing boron penetration during pack boriding (VillaVelázquez-Mendoza et al., 2014; Pacheco et al., 2025).

Surface roughness can alter the effective surface area and diffusion paths for boron atoms. A higher roughness generally increases the number of diffusion sites and may enhance boride layer formation kinetics, while smoother surfaces may reduce diffusion

efficiency due to limited nucleation sites (Ayvaz et al., 2023; Tang et al., 2018).

The surface roughness of maraging steels produced by additive manufacturing, such as Direct Metal Laser Sintering (DMLS) or Selective Laser Melting (SLM), also plays a crucial role in subsequent thermochemical treatments (Bhardwaj & Shukla, 2018). The unique surface topography and microstructural heterogeneity resulting from layer-by-layer melting and rapid solidification can affect both the boriding kinetics and the activation energy values (Casalino et al., 2015; Şirin & Kaynak, 2020).

Furthermore, alloying elements (such as Ni, Mo, and Co in maraging steels) influence both the thermodynamic stability and diffusion coefficients during boride formation, modifying the overall activation energy required for boron diffusion (Kayalı & Kara, 2021). Finally, the boriding process parameters—temperature, time, and boron potential—serve as additional governing factors that determine the activation energy and the resulting microstructural characteristics of the boride layer (VillaVelázquez-Mendoza et al., 2014).

The results for activation energy values of as-built (non-bead blasted) MS1 Maraging Steel and bead blasted MS1 Maraging Steel are summarized in

Table 2. The activation energy values are comparable, indicating no significant difference. Huttunen-Saarivirta et al. stated that higher surface roughness increases surface area and facilitates the coating development process (Huttunen-Saarivirta et al., 2006). In our study, there was not significant change in the activation energies of the two samples. This may be attributed to the fact that the surface roughness of the as-built sample did not change significantly after the glass-bead blasting.

Table 2. Calculated activation energies for all steel samples.

Steel	Activation Energy
Non-Bead Blasted Maraging Steel	**217 kJ/mol**
Bead Blasted Maraging Steel	**222.97 kJ/mol**

Non-bead Blasted Maraging Steel

Figure 10. Square of the boride layer thickness of borided MS1 non-bead blasted maraging steels as a function of process time.

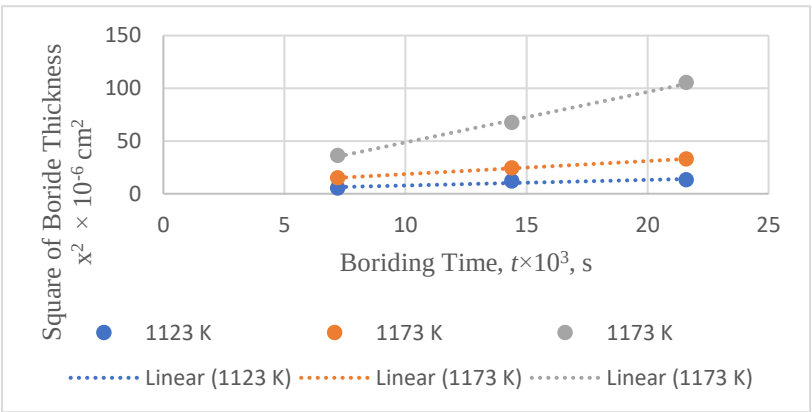

Figure 11: Growth-rate constant versus 1/T graph of borided non-bead blasted MS1 maraging steel.

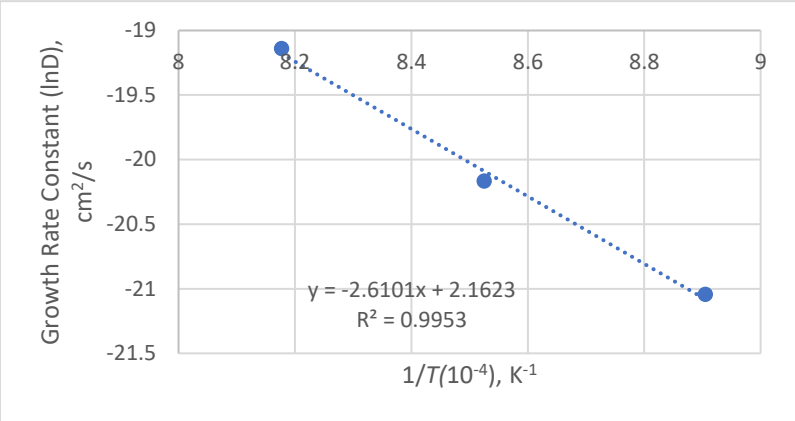

Bead-Blasted Maraging Steel

Figure 12. Square of the boride layer thickness of borided MS1 bead blasted maraging steels as a function of process time.

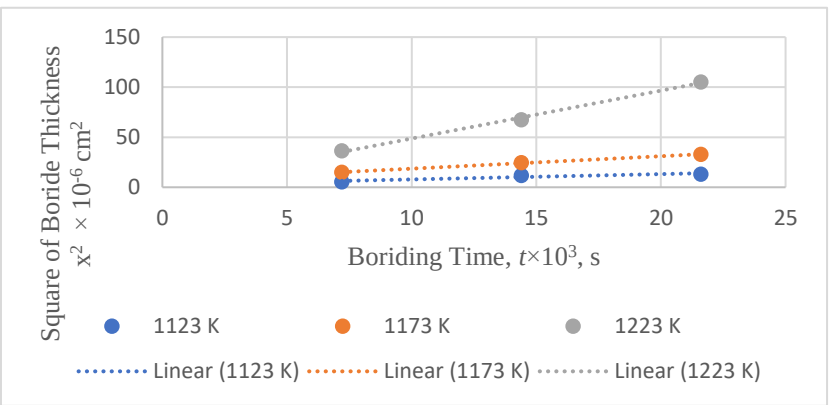

Figure 13. Growth-rate constant versus 1/T graph of borided bead blasted MS1 maraging steel.

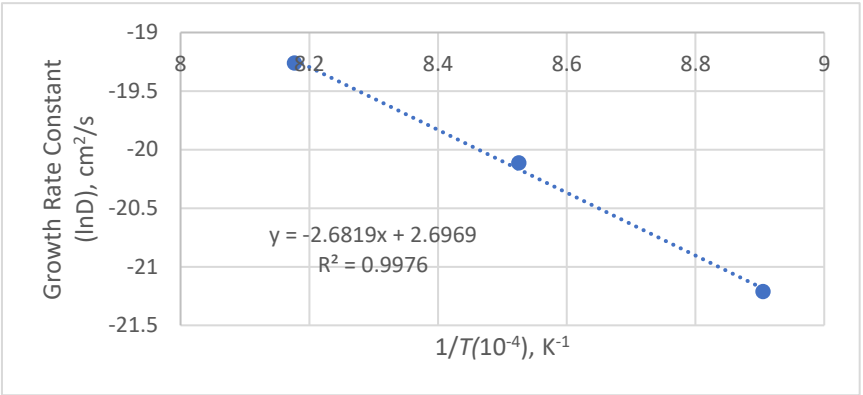

CONCLUSION

In summary, MS1 steel was produced using the Direct Laser Metal Sintering process. The glass bead blasting process was applied to some of the as-built samples and it did not significantly alter the surface roughness (3.4±0.4 µm) of as-built MS1 steel (3.2±0.4 µm). The boriding process of additively manufactured MS1 steel was successfully carried out at the as-built and glass bead-blasted conditions, with the specified temperature and time used for boriding kinetics. As a result, a visible and homogeneous boride layer was obtained. Activation energy calculations for boriding showed that the as-built (217.00 kJ/mol) and glass bead-blasted samples (222.97 kJ/mol) did not result in a significant difference, attributed to the similar surface roughness of both samples.

Acknowledgement

This research was carried out as part of the students' undergraduate theses. Appreciation is extended to ALS Laboratuvar Cihazları Paz. San. ve Tic. Ltd. Şti. for their assistance with the cutting of the samples, and to VEZNELİ Aşındırıcı Sanayi A.Ş. for their support concerning the boriding powder. The project is also supported by the TÜBİTAK 2209-A University Student Research Projects Program under project number 1919B012403178.

References

Ayvaz, S. İ., Aydın, İ., & Bahcepınar, A. İ. (2023). Effect of Shot Blasting on the Boriding Kinetics of AISI 316L Stainless Steel. Protection of Metals and Physical Chemistry of Surfaces, 59(4), 671-678. Doi:10.1134/S2070205123700624

Behl, B., Dong, Y., Pramanik, A., & Bandyopadhyay, T. K. (2025). Evolution of Microstructures and Mechanical Properties of Laser-Welded Maraging Steel for Aerospace Applications: The Past, Present, and Future Prospect. Journal of Manufacturing and Materials Processing, 9(12), 394. Doi:10.3390/jmmp9120394

Bhardwaj, T., & Shukla, M. (2018). Direct metal laser sintering of maraging steel: effect of building orientation on surface roughness and microhardness. *Materials Today: Proceedings, 5*(9), 20485–20491. Doi:10.1016/j.matpr.2018.06.425

Casalino, G., Campanelli, S. L., Contuzzi, N., & Ludovico, A. D. (2015). Experimental investigation and statistical optimisation of the selective laser melting process of a maraging steel. *Optics & Laser Technology, 65*, 151–158. Doi:10.1016/j.optlastec.2014.07.021

Dossett, J., & Totten, G. E. (2013). Steel Heat Treating Fundamentals and Processes. *ASM Handbook, Volume 4A.* içinde ASM International.

Godec, M., Podgornik, B., Kocijan, A., Donik, Č., & Balantič, D. A. S. (2021). Use of plasma nitriding to improve the wear and corrosion resistance of 18Ni-300 maraging steel manufactured by selective laser melting. Scientific Reports, 11(1), 3277. Doi: 10.1038/s41598-021-82572-y

Huttunen-Saarivirta, E., Rohr, V., Stott, F. H., & Schütze, M. (2006). Influence of glass bead blasting of 9% Cr steel substrate on development of aluminide diffusion coatings. *Surface Engineering, 22*(6), 472-480. Doi:10.1179/174327806X124726

Kayalı, Y., & Kara, R. (2021). Investigation of wear behavior and diffusion kinetic values of boronized Hardox-450 steel. *Protection of Metals and Physical Chemistry of Surfaces, 57*(5), 1025-1033. Doi:10.1134/S2070205121050129

Kayali, Y., & Mertgenç, E. (2020). Investigation of diffusion kinetic values of boronized AISI 303 steel by pack boronizing. *Protection of Metals and Physical Chemistry of Surfaces, 56*, 151-155. Doi:10.1134/S2070205120010116

Lawley, A., & Murphy, T. F. (2003). Metallography of powder metallurgy materials. *Materials Characterization, 51*(5), 315–327. Doi:10.1016/j.matchar.2004.01.006

Morel, C., Cioca, V. V., Lavernhe, S., Jardini, A. L., & del Conte, E. G. (2018). Part surface roughness on laser sintering and milling of maraging steel 300. *14th International Conference on High Speed Manufacturing.* https://hal.science/hal-01773243 adresinden alındı

Motallebzadeh, A., Dilektasli, E., Baydogan, M., Atar, E., & Cimenoglu, H. (2015). Evaluation of the effect of boride layer structure on the high temperature wear behavior of borided steels. *Wear, 328*, 110-114. Doi:10.1016/j.wear.2015.01.029

Ozdemir, O., Omar, M. A., Usta, M., Zeytin, S., Bindal, C., & Ucisik, A. H. (2008). An investigation on boriding kinetics of AISI

316 stainless steel. *Vacuum, 83*(1), 175-179. Doi:10.1016/j.vacuum.2008.03.026

Pacheco, C., Jeronimo, J. L., Krelling, A. P., da Costa, C. E., & Milan, J. C. G. (2025). Influence of boriding treatment on the mechanical properties of Monel 400. Results in Surfaces and Interfaces, 18, 100436. Doi:10.1016/j.rsurfi.2025.100436

Tang, L., Jia, W., & Hu, J. (2018). An enhanced rapid plasma nitriding by laser shock peening. Materials Letters, 231, 91-93. Doi:10.1016/j.matlet.2018.08.010

Turk, C., Zunko, H., Aumayr, C., Leitner, H., & Kapp, M. (2019). Advances in maraging steels for additive manufacturing. Berg Huettenmaenn Monatsh, 164(3), 112-6. Doi:10.1007/s00501-019-0835-z

Vander Voort, G. F., ASM International volume 9 (2004)

Doi:10.31399/asm.hb.v09.9781627081771

VillaVelázquez-Mendoza, C. I., Rodríguez-Mendoza, J. L., Ibarra-Galván, V., Hodgkins, R. P., López-Valdivieso, A., Serrato-Palacios, L. L., Leal-Cruz, A. L., & Ibarra-Junquera, V. (2014). Effect of substrate roughness, time and temperature on the processing of iron boride coatings: experimental and statistical approaches. International Journal of Surface Science and Engineering, 8(1), 71-91. Doi: 10.1504/IJSURFSE.2014.059315

Vishwakarma, J., Chattopadhyay, K., & Santhi Srinivas, N. C. (2020). Effect of build orientation on microstructure and tensile behaviour of selectively laser melted M300 maraging steel. Materials Science and Engineering: A, 798, 140130. Doi:10.1016/j.msea.2020.140130

Yapar, U. (2003). Düşük ve orta karbonlu çeliklerin termokimyasal borlama ile yüzey özelliklerinin geliştirilmesi.

BÖLÜM 3

GREEN CHEMISTRY APPROACHES TO PRECIOUS METAL RECOVERY AND NANOPARTICLE SYNTHESIS

1. BURCU NİLGÜN ÇETİNER[1]
2. GÜLAY ARSLAN ÇENE[2]

1. Introduction

The Platinum Group Metals (PGMs) are precious metals with significant worth. According to reports, PGMs are among the most important raw materials in the world. These metals have a major supply problem, given the fact that they are found in scarce amounts in the Earth's crust and are used for a variety of purposes, including catalysis and electronics. Their rarity and the difficulty in replacing them only increase their overall demand. On the other hand, the low-grade reserves of platinum group metals contain a base of sulfur and are of low grade because the high grade ones have been used up. The cost of extracting them, and the impact on the environment do not justify the use of these reserves. Hydrometallurgical techniques are a much greener and cost effective approach as compared to pyro approaches, especially in cases where there are a deficit of platinum and the deposits are of low quality. But

[1] Res. Ass. Dr., Marmara University, Faculty of Engineering, Dept. Of Metallurgical and Materials Eng., Orcid: 0000-0002-3742-4929
[2] Res. Ass. Dr., Marmara University, Faculty of Engineering, Dept. Of Environmental Eng., Orcid: 0000-0003-1983-266X

with the challenges associated with refining platinum, there is a need to find avenues that will reduce waste and retain value (Pianowska et al, 2023; Generowicz, 2022; Sinisalo & Lundström, 2018).

The secondary sources include exhaust automotive catalysts, electronics, scrap electronics, industrial and nuclear spent fuel, military imported goods, jewelry and dental alloys, along with plating solutions used in the jewelry industry, newer chemicals for cancer therapy, and the waste from the deposits of precious metals obtained from ore refineries (Melber et al., 2022; Ravindra et al., 2004; Barakat, 2011; Dean, 1979). Regarding these issues, the platinum group metals – platinum, palladium, and rhodium – have a dramatic significance within catalytic processes in the field of petrochemical technological schemes, particularly in the wide scale. Considering international practice, those metals, which two or three decades ago were exclusively for industrial purposes, now easily find their way into jewelry and other consumer goods owing to the boom in the jewelry trade. Since the early 1980s, the demand for automotive catalysts has profoundly influenced mining operations. The changes in the relatively high value of palladium in the last decade of the 20th century are due to the introduction of systems employing palladium based catalysts that even replaced European three-way catalytic converters. As a result, the primary factors affecting the fluctuation of PGM prices include the advancement of technology, especially in catalysis, that affects the consumption of PGM, as well as the global supply and production cost of PGM (Umeda et al., 2011). Many authors have documented in the literature the use of some components such as concentrated strong acids, bases, and cyanide in classical techniques for the recovery of platinum group metals (PGM) (İlyas et al., 2020; Kim et al., 2010; Mpinga et al., 2014; Quinet et al., 2005; Aktas, 2011; Macrotrends, 2024; Sigma-Aldrich, 2024).

The current trends in the world environment greatly underscore the need to create alternative approaches that are less impactful to the environment and its resources, while at the same time adequately replacing the need to apply hazardous and environmentally damaging chemicals and conventional physical and chemical approaches. Herein, the green chemistry concept stands out particularly because of the main aim to be achieved, which is the use of safe, simple, biodegradable, cost effective, and eco-friendly plants and microorganisms (Sigma-Aldrich, 2024). The increasing focus on the 12 principles of green chemistry, along with greater attention to waste prevention and resource efficiency, leads to the growth of biological and biomimetic approaches to create new advanced materials (Pesen et al., 2023). In the field of sustainability studies, for centuries, cross-regional studies have been carried out on the use of regionally specific agricultural residues in terms of bioenergy and animal feed.

In this way, it can be argued that the appropriate use of biowaste resources contributes to energy generation, environmental protection, and regional economic development, without encroaching on food or animal feed resources (Thirumurugan et al., 2016). The recovery of precious metals and extracting metal ions using the plants' organisms, as this study illustrates, is also a benefit of green chemistry, in addition to the energy and economic value that results from biological wastes. Furthermore, nanobiotechnology requires an inexpensive and environmentally friendly route for the fabrication of metallic nanoparticles. The biological synthesis and characterization of platinum nanoparticles were previously described using extracts from the neem (Azadirachta indica). The gold nanoparticles TEM analysis showed a spherical and microscopic form with a size range of 5 to 50 nm. The results of the FT-IR chloroplatinate ion demonstrated the presence of a protein in the plant that can metamorphose chloroplatinic ion into platinum

nanoparticles (Nayantara, 2018). Their environmental, biotechnological and biomedical application potential is controlled by their size, shape, and spatial arrangement of the fabrication, which determines their physical, chemical, optical, and electronic properties. The synthesis of inorganic metal nanoparticles using wet and dry methods of nanoparticles formation employed several techniques, including ultraviolet, aerosol, lithography, laser ablation, ultrasound, and photochemical reduction.

However, these methods take a toll and require the use of toxic chemicals. Therefore, there is an increasing need for methods that are environmentally friendly. As advances in green chemistry and biological methods occur, there is a demand for simple, low-cost, and environmentally friendly methods. Plants, algae, diatoms, human cell lines, and other biocompatible materials can all synthesize green nanoparticles. These nanoparticles include cobalt, copper, silver, gold, bimetallic alloys, silicon, palladium, platinum, iridium, magnetite, quantum dots, and others. The usage of phototrophic and heterotrophic organisms, as well as biocompatible materials for the synthesis of nanomaterials, is limited by their biodiversity and availability. The present work focuses on the recent trends in the synthesis of green metal nanoparticles and their use in plant systems, aquatic autotrophs, human cell lines, biocompatible materials, and biomolecules (BBC Research, 2024; Mittal, 2014).

According to the estimates, the market for nanoparticles in biotechnology and pharmaceuticals will grow at an average rate of 22.0% from 2014 to 2019, which will result in a total estimated value of $ 79.8 billion by 2019, according to the forecast (BBC Research, 2024; Mittal, 2014), which represents $60.733 billion growth. The structures formed from combining other biocompatible materials, such as proteins, lipids, and polysaccharides, can also achieve this goal. This is due to the relative ease with which they can be combined to construct multilayer drug delivery systems based on

nanotechnology. The biosorbent material, which won this award during the competition and was built by the side of a stream, contains specially functionalized polymers that encapsulate nanoparticles (NPs), which were synthesized by utilizing sol-gel synthesis; the subsequent provision of a low-temperature coating layer resulted in stable particle size and surface charge. Development and progress in drug delivery and targeting systems, in which applications such as nanoparticles and nano-emulsions, which can be targeted to specific areas of the human body that are clinically designed for a specific purpose, are targeted through targeted drug delivery systems. Nanoparticles, over the years, have enormous potential because their unique properties grant them high strength and stability. The biosynthesis methods in broad terms, use polysaccharides, lipids, or proteins as surface stabilizers for the NPs. It has been established that titanium dioxide nanoparticles (TiO_2 NPs) affect seeds' germination, as well as on their viability, partly boosting spinach seeds' germination and the growth of a plant. As micronutrients, metal nanoparticles may be taken up by plants, but increased amounts of these nanoparticles will cause soil pollution. Therefore, it is vital to cut down the levels of metal nanoparticles in soil. Incorporating metallic nanoparticles into biocompatible polymers is beneficial for decreasing dosage levels while increasing potency (Fahmy, 2020).

The beginning of the usage of inorganic nanoparticles dates to about 435 years ago when Paracelsus described the making of aurum potabile, which is known to have minted gold particles (Khandel et al., 2018). Nano compounding has several avenues, which include procedures that are known to be eco-friendly. The production of nanoparticles can be divided into major categories, which include top down strategies and bottom up strategies (Shiraz et al., 2024). In the top down fabrication strategy, bulky materials are broken down into smaller particles, usually less than 100 nm, using

chemical or physical strategies. Top down processes include mechanical processing, laser ablation or cutting, and chemical etching. Although the top down technique can fabricate bulk nanoparticles, the procedure is not ideal in terms of controlling the size, morphology, and purity of the nanoparticles. The bottom-up approach in making nanoparticles makes use of chemical reactions to grow nanoparticles by combining atoms, molecules, or ions. This makes it possible to control various characteristics of the results, including size, structure, and purity of the nanoparticles made. Bottom up methods include but are not limited to sol-gel, hydrothermal, and chemical vapor deposition. It is in this respect that, of late, there has been a steady but aggressive growth of new ideas and possibilities in green chemistry, especially in the subsections that seek to synthesize metallic nanoparticles.

Among them, the elements gold (Au), silver (Ag), lead (Pb), platinum (Pt), copper (Cu), iron (Fe), cadmium (Cd), magnesium (Mg), silicon (Si), cobalt (Co), titanium (Ti), tantalum (Ta), vanadium (V), chromium (Cr), manganese (Mn), zinc (Zn), niobium (Nb), barium (Ba), cesium (Cs), tungsten (W), palladium (Pd), and rhodium (Rh) are particularly notable. The synthesis of nanoparticles and Re (ruthenium) & In (indium) metal oxides such as titanium oxide and zinc oxide has also been studied in detail mostly using chemical physical and biological approaches including the use of microorganisms (Shiraz et al., 2024; Khandel et al., 2018; Şahin et al., 2018). As with human beings, various parts of a plant can also be subjected to a synthesis process, including leaves, flowers, roots, and stems. Additionally, biomolecules like proteins, sugars, lipids, and carbohydrates, as well as coenzymes can be employed. For instance, in the case of the plant-based additive, consisting of biopolymers that reduce metals, the ion to nanoparticle conversion is decreased when bio composite nanomaterials are synthesized via plants or plant parts, including leaves, stems, and roots. The reduction of the metal

ions is mediated by the plant, which is an effective route that is also inexpensive and some would argue, the most practical. The extract of a plant comprises bioactive compounds like the class of polyphenols flavonoids which contribute to the thermal stability of the particulate formed, and the terpenoids and alkaloids are well documented to hinder or assist in the process of forming the foundation for nanoparticles (Şahin et al., 2018; Nishanthi et al., 2019; Al-Radadi, 2019).

Cost-effectiveness, ease of use, and the ability to produce differently shaped nanoparticles are some of the benefits of plant mediated synthesis. The first synthesis of green routes that employs plant material is the least harmful and most eco-friendly one. Synthesis from plants that are available at hand has great cost benefits and is simple to execute. Plants not only remove metal contaminants but also mitigate, detoxify, and sequester the metals. Phytochemicals, which include anthocyanins, polyphenols, or even alkaloids in plants, act as reducing and capping agents during green synthesis of metallic nanoparticles either extracellularly or intracellularly. It is possible to synthesize stable nanoparticles using a variety of herbs and extracts in a single container. This method of producing gold and silver nanoparticles was the first to be developed. It is reported that aloe vera, neem (Azadirachta indica), lemongrass, sunflower, alfalfa, and other widely available plants have been used to make metal nanoparticles, including silver, copper, cobalt, and zinc. Alfalfa roots can take up Ag(0) from agar and may be responsible for its distribution within the plant. Silver ion was shown to reduce in the leaf extract of the Pelargonium graneolens (Şahin et al., 2018; Nishanthi et al., 2019; Al-Radadi, 2019; Eltaweil et al., 2022; Bartolucci et al., 2020; Eltaweil et al., 2022).

Extracellular polysaccharides produced by biological systems can concurrently decrease metal ions and stabilize the

creation of pure metallic silver (Ag), gold (Au), or bimetallic nanoparticles. Specifically, extracellular nanoparticles synthesized from the leaf extract of Azadirachta indica preserve the functional properties of polysaccharides, serving as both reducing and capping agents. Due to these characteristics, numerous plant species have been investigated for the eco-friendly synthesis of metal nanoparticles designed for use as medical preservatives. Gold nanoparticles measuring between roughly 50 and 100 nm are extensively researched for their distinctive physicochemical characteristics. The manufacture of monomeric gold nanoparticles often necessitates the reduction of gold precursors with a potent reducing agent like sodium borohydride ($NaBH_4$), typically performed in an organic solvent such as acetone to regulate nucleation and development. Ganji developed a compelling technique designed to enhance the functional range and stability of nanomaterials, especially in intricate biological contexts. This method involves encapsulating enzymes within a gold-silicate shell, which enhances their stability in cytosolic environments. The research highlighted that the chemical composition, as well as the size, shape, and thickness of the infiltrated gold-silicate clusters, are crucial for attaining high structural stability (Şahin et al., 2018; Nishanthi et al., 2019; Al-Radadi, 2019; Eltaweil et al., 2022; Bartolucci et al., 2020; Eltaweil et al., 2022).

Currently, gold nanoshells are mainly synthesized using macromolecular templating strategies and light-assisted fabrication techniques, which allow precise control over shell thickness, morphology, and optical properties. These advances represent significant progress in the development of functional nanomaterials for biomedical and environmental applications. In parallel, plant- and biomass-derived polymers rich in polyols, carboxylic groups, and galacturonic acid derivatives have gained increasing attention as natural stabilizers and reducing agents in green nanomaterial

synthesis. Their biocompatibility, abundance, and ability to provide functionalized surfaces enable synergistic integration of biological extracts within polymeric matrices, supporting the development of sustainable composite nanomaterials for diverse technological applications (Şahin et al., 2018; Nishanthi et al., 2019; Al-Radadi, 2019; Eltaweil et al., 2022; Bartolucci et al., 2020; Eltaweil et al., 2022).

Green synthesis methods have been extensively investigated for the fabrication of noble metal nanoparticles. Nanoparticles synthesized in the presence of terpenes and reducing sugars from Ocimum sanctum (tulsi) frequently display chaotic geometries. Platinum nanoparticles have been effectively generated utilizing fungal species such as Fusarium oxys porum and Neurospora crassa, underscoring the potential of microorganisms as proficient biogenic reducing agents (Shiraz et al., 2024). Platinum nanoparticles sourced from plants such as Anogeissus latifolia and Dioscorea bulbifera exhibit unique optical characteristics, varied nanostructures, and superior catalytic efficacy, making them highly appropriate for industrial reduction reactions.

Recent advancements have broadened the variety of natural materials utilized in the manufacture of platinum nanoparticles. These encompass plant- and biomass-derived sources like Pinus resinosa, Diospyros kaki (persimmon), Taraxacum laevigatum (red-seeded dandelion), Nigella sativa, Ononis spinosa, tea polyphenols, water hyacinth, garden mint, pomegranate, cashew leaves, and Bacopa monnieri. The literature identifies additional plant sources including Dioscorea bulbifera tubers, green tea powder, Maytenus royleanus, Prunus × yedoensis, Platycladus orientalis shoots, Quercus glauca, Garcinia mangostana, and Atriplex halimus (saltbush) (Şahin et al., 2018; Nishanthi et al., 2019; Al-Radadi, 2019; Eltaweil et al., 2022; Bartolucci et al., 2020; Eltaweil et al., 2022).

In addition to catalytic applications, these biogenically produced nanoparticles have garnered significant interest for medicinal and environmental purposes, such as wastewater treatment, medication delivery systems, diagnostic instruments, and imaging applications. Platinum nanoparticles made using green-synthesis methods have been shown to have multiple uses in various fields of research (Shiraz et al., 2024).

- Platinum nanoparticles have a large range of applications in chemical reactions owing to their high catalytic activity. Such materials are also used for the catalytic transformation of toxic gases such as carbon monoxide into carbon dioxide and in chemical synthesis.
- Because of their small size, high surface area, and biocompatibility, platinum nanoparticles are suitable for use in cancer treatments, drug delivery, and imaging. They act as drugs and other therapeutic agents, making them useful in photodynamic therapy for cancer treatment.

Studies show that nanoparticles of gold and platinum produced using the plant extracts exhibit notable wound healing and tissue regeneration effects due to anti-inflammatory effects. It can be concluded that gold and platinum nanoparticles can suppress inflammation naturally (Şahin et al., 2018). Moreover, other plant-derived nanoparticles, such as gold, platinum, palladium, and silver have worked in controlling the malaria population in the environment (Şahin et al., 2018).

- There is potential for platinum nanoparticles to enhance the process of environmental cleaning by breaking down the pollutants present in the contaminated water and soil. This integrated process may remove the hazardous metals and organic chemicals contained in industrial effluents and soil.

- Platinum nanoparticles are found in a wide range of devices used for energy conversion and energy storage, such as fuel cells, batteries, and solar cells, where they enhance overall device efficiency.
- Platinum-based green-synthesized nanoparticles are increasingly incorporated into sensing and monitoring platforms due to their high surface activity, stability, and selectivity. These nanomaterials have been utilized in the development of gas sensors, biosensors, and environmental monitoring devices, significantly improving detection sensitivity and analytical performance.

Moreover, the benefits of green nanoparticle synthesis encompass the use of plant-derived chemicals as dual reducing and stabilizing agents, facilitating the generation of stable nanoparticles without requiring additional physicochemical processing processes. Plant extracts contain abundant bioactive phytochemicals, including flavonoids, phenolic compounds, citric acid, ascorbic acid, polyphenols, terpenes, alkaloids, enzymes, and proteins, which together facilitate metal ion reduction and nanoparticle stability (Nishanthi et al., 2019).

Notwithstanding these benefits, plant-mediated synthesis methods nevertheless exhibit specific constraints. Diversity in plant species, plant components, growth circumstances, and extraction methodologies frequently results in inadequate regulation of nanoparticle dimensions and morphological consistency. Moreover, difficulties associated with extraction, isolation, and purification, coupled with very low synthesis and recovery efficiency, may impede large-scale use. A comprehensive understanding of the selection of suitable plant extracts and the fundamental reduction and stabilization mechanisms is crucial for attaining reproducible and regulated nanoparticle manufacturing. Understanding how nanoparticles are synthesized in vivo is crucial for the rational

development of industrial methods for the synthesis of nanoparticles, which have desirable physicochemical properties, high biological activity, and low toxicity (Bartolucci et al., 2020). It describes the assessment of the plant system for the green biosynthesis of nanoparticles employing an easy and reliable technique. Several plant parts like Argemona mexicana, chickpea, lemongrass, black pepper, neem, and mango have been found to use the metabolism within the cell for the conversion of Au (III) ions to form gold biomolecules and alter silver ions to gold nanoparticles. Also, sorbents from plants have been created. Among the works carried out in our country are the adsorption of Ni(II) with a new activated carbon made from grape pomace (Orhan & Erdem, 2017), adsorption of dye Basic Blue 3 by pinecones (Tanyıldızı & Uygut, 2016), adsorption of citric acid modified and activated sugar beet pulp (MSBP) for the removal of Pb (II) and Cd(II) ions from aqueous solutions (Arslanoğlu & Tümen, 2015).

The distinctiveness of the lithium–sulfur (Li–S) battery system is in its remarkably high theoretical energy density, surpassing that of traditional lithium-ion batteries. Despite considerable advancements in tackling electrochemical issues, the creation of affordable, eco-friendly sulfur host materials that can enable the reversible transformation between sulfur and polysulfides is essential for practical application. Biomass-derived carbon compounds have garnered heightened interest owing to their sustainability, adjustable porosity, and capacity for heteroatom doping. Recent research indicate that chickpea-derived biomass can function as a multifaceted platform for the production of sophisticated materials. Cobalt nanocrystals have been synthesized on a gram scale utilizing three-dimensional porous nitrogen-doped mesoporous carbon templates derived from pressure-assisted carbonization of chickpeas (Faheem et al., 2021). In addition to energy-related uses, chickpea-based systems have been investigated

for the synthesis of green nanomaterials. Silver nanoparticles (AgNPs) have been effectively produced utilizing aqueous leaf extracts of chickpea (Cicer arietinum L.), wherein plant-derived biomolecules function as both reducing and stabilizing agents (Baran et al., 2022). Likewise, chickpea leaf exudates have been employed in the production of benzopyran derivatives, underscoring the rich phytochemical potential of this biomass (Snehali et al., 2018).

The structural carbon content of chickpea shells has facilitated their utilization as a precursor to produce multi-walled carbon nanotubes, highlighting the promise of chickpea-derived materials as sustainable carbon sources for nanostructured applications (Singh et al., 2021). This research collectively demonstrates the multifaceted significance of chickpea biomass as a sustainable precursor for energy storage, nanomaterial synthesis, and the generation of useful organic compounds. Using plants for green nanotechnology metabolism is an innovative approach of using flora that relates with the value addition of metals, by reducing and recovering them into active simple nanoparticles. By using this method, the use of toxic chemicals within the process will be reduced, which is better for the environment. In addition, new techniques for recovering platinum group metals (PGM) and other precious metals using this method became possible and inexpensive.

The bio-reducing materials of greatest interest in green synthesis are plant extracts. Recently, hydroalcoholic extracts of Cistus ladanifer, Erica andevalensis and Rubus idaeus species were found to precipitate palladium and platinum in leachates. These methods can recover over 60% which shows prospecting as substitutes for conventional chemical processes (Nobahar et al., 2023). Moreover, green synthesis methods involve the utilization of plant extracts as reducing and stabilizing agents for the production of gold and palladium nanoparticles, while alkanethiol self-assembled monolayers are used to modify surface functionality and

improve nanoparticle stability. The incorporation of these eco-friendly techniques facilitates the production of noble metal nanoparticles under moderate circumstances, obviating the necessity for harmful reagents and promoting sustainable nanomaterial design (Martínez-Barbosa & Figueroa-Pizano, 2024; Kandav & Sharma, 2023).

Phytoremediation facilitates eco-friendly synthesis methods by utilizing hyperaccumulator plants to extract heavy metals from polluted soils and aquatic environments. Processes like phytoextraction and rhizofiltration facilitate the effective absorption and accumulation of metals in plant biomass, yielding a sustainable metal-enriched feedstock for future green synthesis methods. Subsequent to metal absorption, post-treatment methods such as composting and heat processing can augment biomass valorization by enabling the extraction of important metals and bioactive compounds. This comprehensive strategy enhances the environmental efficacy of remediation operations and aids in resource recovery in an environmentally friendly fashion (Tan et al., 2023). Integrating phytoremediation with green synthesis efficiently actualizes the concepts of the circular economy, converting waste-derived biomass into value-added products. When it comes to green synthesis, the socio-economic and ecological gains are immense. This is due to its ability to fit within the framework of sustainable development goals in terms of lower environmental footprints, involvement of non-toxic solvents and low waste. Furthermore, it provides considerable savings in production costs over traditional approaches, promoting a wideness of applications. For example, on account of decreased cost of nanoparticle production, green synthesis is poised to be one of the viable options in the industrial and environmental arena (Kandav & Sharma, 2023).

With all its merits, green synthesis has pitfalls as well, one of the most significant being the washing off contaminants during

phytoremediation, causing a secondary pollution problem. The solution to these challenges would involve modern process design, which would improve the effectiveness and forecasting of such recovery strategies through the fusion with artificial intelligence technologies. In the future, research should concentrate on resolving these bottlenecks so that this new method of eco-friendly metal recovery can be applied on a large scale.

In this chapter, we first review conventional and green approaches for recovering platinum group metals from secondary resources. We then focus on plant-mediated and other biological routes for the green synthesis of noble metal nanoparticles, with particular emphasis on platinum-based systems. Finally, we discuss scale-up challenges, environmental considerations, and future perspectives linking precious metal recovery with green nanotechnology and environmental remediation.

Plant-based synthesis of nanoparticles and scale-up challenges

The synthesis of nanoparticles through plants has garnered interest as a nonharmful method of fabricating materials, as it employs the biochemical metabolism of plants for both reduction and stabilization of such materials. Yet, process intensification of these systems to enhance industrial deployment indicates new avenues of complexity, including industrial reproducibility, economic cost, and quality assessment. This chapter aims to provide perspectives from the recent literature on the technological development and scale-up of plant-based nanoparticle synthesis.

It has been noted that one of the major obstacles inhibiting the use of nanoparticles in industry is the consistent production of the same properties of the particles. Research on plant extracts by Strieder et al. (2024) highlights the difficulty posed by mass production on supra-molecular properties due to the different constituents of plant extracts in relation to the production of

nanoparticles with uniform shape and size. In conclusion, the authors argue that the standardization of the conditions under which plants are cultivated and the conditions under which the nano particles are extracted, would resolve these inconsistences thereby enhancing the uniform production of nano particles at an economically advantageous scale. Also, Duarte et al. (2020) showed that the use of active constituents of agribusiness waste in various reaction volumes of nano reactive materials made it likely to maintain the size and encapsulation ratio, indicating the possibility of performing up scaling under optimal thermal reaction bounds.

Cost efficiency is another critical barrier to industrialization. Research by Fernandes et al. (2023) highlights the economic issues that the existing methods of producing nanoparticles pose, that is, high energy cost and material waste. A top-down and bottom up approach, though effective on miniatures, encounters problems like coarse aggregates and contamination during scaling up. Some progress has been made in the microfluidizer and supercritical fluid technologies, which offer better controls on the size and distribution of particles at cheaper costs, as discussed in Patel et al. (2021). These methods have great potential to circumvent the problems experienced in attempting to translate laboratory scale synthesis to the industrial scale.

While environmental sustainability is a core aspect of the green synthesis philosophy, large-scale implementations tend to disregard this principle. Avoidable secondary pollutions like plant residue, solvents, and other substances should be properly managed. Silva et al. (2015) suggest measures such as raw material by-products reuse and closed-loop systems, which may help reduce the environmental impacts during scaled-up synthesis of nanoparticles. Their work demonstrates the need to ensure that industrial processes are compatible with green chemical approaches, so that scale-up can achieve desired outcomes without putting the environment at risk.

To sum up, the challenges about reconciling reproducibility, economic optimization, and environmental considerations determine the conversion of plant-based nanoparticles on a larger scale for use in various industries. Recent research suggests that some of these difficulties can be overcome by incorporating innovations in extraction protocols, new facilities, and environmentally friendly technologies. By empowering such developments, the realm has the capacity to transform industries such as agriculture and medicine, offering affordable, readily available, and environmentally friendly alternatives to nanomaterials for the world at large.

The utilization of plant-derived nanoparticles in environmental remediation is gaining traction as an innovative and sustainable solution to pollution challenges. These nanoparticles, synthesized through eco-friendly processes using plant extracts, offer unique advantages such as biocompatibility, reduced environmental impact, and enhanced efficiency in removing contaminants from water, air, and soil. By aligning with the principles of green chemistry, plant-based synthesis provides a path toward achieving global sustainability goals.

Plant-based nanoparticles have proven effective in removing both organic and inorganic pollutants through advanced remediation techniques, including adsorption, catalysis, and membrane filtration. For instance, algae-based nanoparticles have demonstrated catalytic activity against organic contaminants like dyes and phenols, offering a cost-effective and sustainable alternative to traditional methods (Premarathna et al., 2025). Similarly, the use of magnetic copper ferrite nanoparticles immobilized on rice husk-derived zeolite has shown significant success in adsorbing chlorogenic acid, achieving over 89% removal efficiency within an hour (Neves et al., 2025).

These studies highlight the potential of utilizing agro-industrial waste and plant byproducts for environmental remediation. Beyond

their effectiveness, the scalability and circular economic potential of plant-derived nanoparticles present a compelling case for their adoption. Researchers have highlighted how materials such as rice husk and algae not only act as reducing agents but also contribute to creating value-added products from agricultural waste, aligning with circular economic principles. Furthermore, green nanoparticles have shown enhanced performance in wastewater treatment applications by improving pollutant adsorption and antifouling properties in membrane technologies (Somya, 2025).

Despite their promise, challenges remain in scaling up plant-based nanoparticle synthesis for industrial applications. Issues such as variability in plant extract composition, stability of nanoparticles, and the risk of secondary pollution during large-scale production must be addressed. Kapoor et al. (2024) stress the importance of developing standardized protocols and adopting life cycle analysis to mitigate these challenges while ensuring sustainability in production and application (Kapoor et al., 2024). Additionally, advancements in artificial intelligence and machine learning could play a crucial role in optimizing synthesis parameters and predicting performance outcomes for various environmental scenarios.

In conclusion, plant-derived nanoparticles represent a sustainable and innovative approach to environmental remediation. By harnessing renewable biological resources and integrating circular economy principles, this method offers a viable solution to addressing global pollution challenges. Continued research and interdisciplinary collaboration are essential to overcoming scalability and implementation hurdles, paving the way for broader industrial adoption and more resilient environmental practices.

References

Aktas, S. (2011). Rhodium recovery from rhodium-containing waste rinsing water via cementation using zinc powder. *Hydrometallurgy*, *106*(1-2), 71-75.

Al-Radadi, N. S. (2019). Green synthesis of platinum nanoparticles using Saudi's Dates extract and their usage on the cancer cell treatment. Arabian Journal of Chemistry, 12, 330–349. https://doi.org/10.1016/j.arabjc.2018.05.008.

Arslanoğlu, H., & Tümen, F. (2015). Sitrik asitle modifiye edilmiş şeker pancarı küspesi ile sulu çözeltilerden Pb(II) ve Cd(II) giderilmesi. Fırat Üniversitesi Mühendislik Bilimleri Dergisi, 27(1), 85-99.

Barakat, M. A. (2011). New trends in removing heavy metals from industrial wastewater – Review article. Arabian Journal of Chemistry, 4, 361–377. https://doi.org/10.1016/j.arabjc.2010.07.019

Baran, A., Baran, M. F., Keskin, C., Hatipoğlu, A., Yavuz, Ö., İrtegün Kandemir, S., Adican, M. T., Khalilov, R., Mammadova, A., Ahmadian, E., Rosić, G., Selakovic, D., & Eftekhari, A. (2022). Investigation of antimicrobial and cytotoxic properties and specification of silver nanoparticles (AgNPs) derived from Cicer arietinum L. green leaf extract. Frontiers in Bioengineering and Biotechnology, 10, 855136.

Bartolucci, C., Antonacci, A., Arduini, F., Moscone, D., Fraceto, L., Campos, E., Attaallah, R., Amine, A., Zanardi, C., Cubillana-Aguilera, L. M., Santander, J. M. P., & Scognamiglio, V. (2020). Green nanomaterials fostering agrifood sustainability. Trends in Analytical Chemistry, 125, 115840.

BCC Research. (2024). Nanoparticles in biotechnology, drug development, and drug delivery. Retrieved September 13, 2024, https://www.bccresearch.com/marketresearch/biotechnology/nanop

articles-biotechnology-drug-development-drug-delivery-report.html.

Dean, J. A. (1979). Lange's handbook of chemistry (12th ed.). McGraw-Hill Inc.

de Moura Strieder, C., Macuvele, D. L. P., Soares, C., Padoin, N., & Riella, H. G. (2024). Plant-mediated green synthesis of cerium oxide nanoparticles: a critical perspective of some unclear issues. *Journal of Materials Research and Technology*, *30*, 6376-6388.

Duarte, D. S., Nascimento, J. A. D. A., & Britto, D. D. (2020). Scale-up in the synthesis of nanoparticles for encapsulation of agroindustrial active principles. *Ciência e Agrotecnologia*, *43*, e023819.

Eltaweil, A. S., Fawzy, M., Hosny, M., Abd El-Monaem, E. M., Tamer, T. M., & Omer, A. M. (2022). Green synthesis of platinum nanoparticles using Atriplex halimus leaves for potential antimicrobial, antioxidant, and catalytic applications. Arabian Journal of Chemistry, 15, 103517.

Faheem, M., Li, W., Ahmad, N., Yang, L., Tufail, M. K., Zhou, Y., Zhou, L., Chen, R., & Yang, W. (2021). Chickpea derived Co nanocrystal encapsulated in 3D nitrogen-doped mesoporous carbon: Pressure cooking synthetic strategy and its application in lithium-sulfur batteries. Journal of Colloid and Interface Science, 585, 328–336. https://doi.org/10.1016/j.jcis.2020.11.050.

Fahmy, S. A., Preis, E., Bakowsky, U., & Azzazy, H. M. E. S. (2020). Platinum nanoparticles: green synthesis and biomedical applications. *Molecules*, *25*(21), 4981.

Fernandes, C., Jathar, M., Sawant, B. K. S., & Warde, T. (2023). Scale-up of nanoparticle manufacturing process.

In *Pharmaceutical process engineering and scale-up principles* (pp. 173-203). Cham: Springer Nature Switzerland.

Generowicz, N. The Importance of Recovery of PGMS from Catalysts – A Case Study of Recycling Network in Poland. Architecture, Civil Engineering, Environment, 2022, Sciendo, vol. 15 no. 2, pp. 149-156. https://doi.org/10.2478/acee-2022-0022.

Ilyas, S., Srivastava, R. R., Kim, H., & Cheema, H. A. (2020). Hydrometallurgical recycling of palladium and platinum from exhausted diesel oxidation catalysts. Separation and Purification Technology, 248, 117029.

Kandav, M., & Sharma, P. (2023). Green nanotechnology: Plant-mediated synthesis of metal nanoparticles and applications. Materials Today Communications, 26, 102456. https://doi.org/10.1016/j.mtcomm.2023.102456.

Kapoor, N., et al. (2024). Nano-resolutions for Environmental Salvation: Leaping to Sustainability. Current Green Chemistry. DOI: 10.2174/0122133461351615241104145045

Khandel, P., Yadaw, R. K., Soni, D. K., Kanwar, L., & Shahi, S. K. (2018). Biogenesis of metal nanoparticles and their pharmacological applications: Present status and application prospects. Journal of Nanostructure in Chemistry, 8, 217–254. https://doi.org/10.1007/s40097-018-0267-4

Kim, M., Kim, E., Jeong, J., Lee, J., & Kim, W. (2010). Recovery of platinum and palladium from the spent petroleum catalysts by substrate dissolution in sulfuric acid. Materials Transactions, 51(10), 1927–1933. https://doi.org/10.2320/matertrans.M2010218.

Macrotrends. (2024). Platinum prices historical chart data. Retrieved September 13, 2024, from

https://www.macrotrends.net/2540/platinum-prices-historical-chart-data

Martínez-Barbosa, N., & Figueroa-Pizano, M. (2024). Advances in green synthesis of metallic nanoparticles using plant-based extracts. Environmental Nanotechnology, Monitoring & Management, 12, 102431.

Melber, C., Keller, D., & Mangelsdorf, I. (2002). Palladium: Environmental health criteria. World Health Organization.

Mittal, J., et al. (2014). Phytofabrication of nanoparticles through plants as nanofactories. Advances in Natural Sciences: Nanoscience and Nanotechnology, 5, 043002.

Mpinga, C. N., Bradshaw, S. M., Akdogan, G., Snyders, C. A., & Eksteen, J. J. (2014). Evaluation of the Merrill–Crowe process for the simultaneous removal of platinum, palladium and gold from cyanide leach solutions. Hydrometallurgy, 142, 36–46. https://doi.org/10.1016/j.hydromet.2013.11.004.

Nayantara, P. K. (2018). Biosynthesis of nanoparticles using eco-friendly factories and their role in plant pathogenicity: A review. Biotechnology Research and Innovation, 2, 63-73. https://doi.org/10.1016/j.biori.2018.09.003.

Neves, T. R., Schildt, L. F. L., Silva, M. L. L. S. E., Vasconcelos, V. V. V., Di Conzo, C., Mura, F., & Paris, E. C. (2024). Magnetic CuFe2O4 Nanoparticles Immobilized on Modified Rice Husk-Derived Zeolite for Chlorogenic Acid Adsorption. Magnetochemistry, 10(11), 87.

Nishanthi, R., Malathi, S., John Paul, S., & Palani, P. (2019). Green synthesis and characterization of bioinspired silver, gold and platinum nanoparticles and evaluation of their synergistic antibacterial activity after combining with different classes of

antibiotics. Materials Science & Engineering C, 96, 693–707. https://doi.org/10.1016/j.msec.2018.11.050.

Nobahar, A., Martínez-Barbosa, N., & Figueroa-Pizano, M. (2023). Hydroalcoholic extracts for platinum group metal recovery: Advances and challenges. Journal of Cleaner Production, 410, 136456. https://doi.org/10.1016/j.jclepro.2023.136456.

Orhan, R., & Erdem, M. (2017). Üzüm sapından hazırlanan aktif karbon ile sulu çözeltilerden Ni(II)'nin giderimi. Fırat Üniversitesi Mühendislik Bilimleri Dergisi, 29(1), 319-324.

Patel, D. M., Patel, N. N., & Patel, J. K. (2021). Nanomedicine scale-up technologies: feasibilities and challenges. In *Emerging technologies for nanoparticle manufacturing* (pp. 511-539). Cham: Springer International Publishing.

Pesen, D., Gençay, G., & Kurşun, B. (2023). Environmental and economic analysis of bioenergy production and utilization in Adana, Turkey. Celal Bayar University Journal of Science, 19(1), 1-10. https://doi.org/10.18466/cbayarfbe.1175413.

Pianowska, K., Kluczka, J., Benke, G., Goc, K., Malarz, J., Ochmański, M., & Leszczyńska-Sejda, K. (2023). Solvent Extraction as a Method of Recovery and Separation of Platinum Group Metals. Materials, 16(13), 4681. https://doi.org/10.3390/ma16134681.

Premarathna, K. S. D., Lau, S. Y., Chiong, T., Show, P. L., Vithanage, M., & Lam, M. K. (2025). Greening up the fight against emerging contaminants: algae-based nanoparticles for water remediation. *Clean Technologies and Environmental Policy*, *27*(10), 5825-5842.

Ravindra, K., Bencs, L., & Van Grieken, R. (2004). Platinum group elements in the environment and their health risk. Science of

the Total Environment, 318, 1–43. https://doi.org/10.1016/S0048-9697(03)00372-3.

Shiraz, M., Imtiaz, H., Azam, A., et al. (2024). Phytogenic nanoparticles: Synthesis, characterization, and their roles in physiology and biochemistry of plants. Biometals, 37, 23–70. https://doi.org/10.1007/s10534-023-00542-5.

Sigma-Aldrich. (2024). Green chemistry. Retrieved September 13, 2024, from https://www.sigmaaldrich.com/chemistry/greener-alternatives/green-chemistry.html.

Silva, L. P., Reis, I. G., & Bonatto, C. C. (2015). Green synthesis of metal nanoparticles by plants: current trends and challenges. *Green processes for nanotechnology: from inorganic to bioinspired nanomaterials*, 259-275.

Singh, V., Chatterjee, S., Palecha, M., Sen, P., Ateeq, B., & Verma, V. (2021). Chickpea peel waste as sustainable precursor for synthesis of fluorescent carbon nanotubes for bioimaging application. Carbon Letters, 31, 117–123.

Sinisalo, P. and Lundström, M. (2018). Refining approaches in the platinum group metal processing value chain—a review. Metals, 8(4), 203. https://doi.org/10.3390/met8040203.

Snehali, M., Sachin, S., Shashikant, D., & Suresh, P. (2018). Synergistic effect of natural chickpea leaf exudates acids in heterocyclization: A greener protocol for benzopyran synthesis. Royal Society Open Science, 5(1), 170333. https://doi.org/10.1098/rsos.170333.

Somya, A., et al. (2024). Green nanoparticles. In Advances in Chemical and Materials Engineering. IGI Global. https://doi.org/10.4018/979-8-3693-6240-2.ch004.

Şahin, B., Aygün, A., Gündüz, H., Şahin, K., Demir, E., Akocak, S., & Şen, F. (2018). Cytotoxic effects of platinum nanoparticles obtained from pomegranate extract by the green synthesis method on the MCF-7 cell line. Colloids and Surfaces B: Biointerfaces, 163, 119-124. https://doi.org/10.1016/j.colsurfb.2017.12.042.

Tan, X., Wang, J., & Zhao, L. (2023). Advances in phytoremediation for heavy metal recovery. Journal of Environmental Management, 316, 115432. https://doi.org/10.1016/j.jenvman.2023.115432.

Tanyıldızı, M. Ş., & Uygut, M. A. (2016). Çam kozalağıyla bazik mavi 3 adsorpsiyonu. Fırat Üniversitesi Mühendislik Bilimleri Dergisi, 28(2), 169-174.

Thirumurugan, A., Aswitha, P., Kiruthika, C., Nagarajan, S., & Nancy Christy, A. (2016). Green synthesis of platinum nanoparticles using Azadirachta indica – An eco-friendly approach. Materials Letters, 170, 175–178. https://doi.org/10.1016/j.matlet.2016.02.026.

Umeda, H., Sasaki, A., Takahashi, K., Haga, K., Takasaki, Y., & Shibayama, A. (2011). Recovery and concentration of precious metals from strong acidic wastewater. Materials Transactions, 52(7), 1462–1470. https://doi.org/10.2320/matertrans.M2010432.

Quinet, P., Proost, J., & Van Lierde, A. (2005). Recovery of precious metals from electronic scrap by hydrometallurgical processing routes. Minerals and Metallurgical Processing, 22(1), 17-22. https://doi.org/10.1007/BF03403191.

BÖLÜM 4

A REVIEW OF RECENT DEVELOPMENTS IN NEW GENERATION BIODEGRADABLE CU ADDED ZN ALLOYS DESIGNED FOR ORTHOPEDIC APPLICATIONS

1. HALİL EREN[1]

Introduction

Orthopedic implant materials are required for the repair of bone fractures. The types and materials of implants are selected based on the characteristics of the broken bones. Generally, bioinert metal alloys are used as implant materials for bone repair. However, the use of these materials can cause some negative consequences (Hussain et al., 2023). Examples of these include osteoporosis, bone necrosis, delayed bone healing, or inflammation, etc. In addition to these, the need for secondary surgeries to remove the implants is also a major problem. Because this situation presents both extra costs and procedural risks for patients (Hussain et al., 2023).

Stainless steels or titanium materials are traditionally used as bone implant materials due to their high durability. New generation materials are being developed to overcome the challenges posed by

[1] Lecturer Dr., Çankırı Karatekin University, Materials and Materials Processing Technologies Department, Orcid: 0000-0002-4224-683X

these materials. Biodegradable metal alloys have garnered particular attention in recent years due to both their strength and degradability (Wu et al. 2025; Li et al. 2020). Mg alloys were approved by the Food and Drug Administration, United States, in March 2023 as a biodegradable metal implant material (Wu et al. 2025). In addition to having sufficient mechanical strength, they need to be developed due to high corrosion rates. At the same time, the release of hydrogen gas produced during the degradation of these alloys also causes tissue damage, delaying tissue regeneration (Wu et al. 2025).

In recent years, studies on biodegradable metal alloys have focused on Zn alloys. Because these alloys do not release as much hydrogen during decomposition as Mg alloys do. At the same time, corrosion rates are lower compared to Mg alloys. For these two reasons, Zn alloys are attracting attention as biodegradable next-generation alloys (Wu et al. 2025; Li et al. 2020). At the same time, the positive effect of Zn2+ ions on bone formation is also increasing interest in Zn alloys (Wu et al. 2025; Qiao et al.2022). Alloying plays a significant role in increasing the durability of the Zn element. Elements such as Cu, Sr, Ag, Mn, Se, Li, and Mg can be used in Zn alloys (Yang et al. 2025). With elements, about 2-3 mg can be taken into the body per day. This is one of the reasons why it is used as a biodegradable additive element (Yang et al. 2025). In addition, copper exhibits excellent antibacterial effects to prevent inflammation (Yang et al. 2025; Shuai et al. 2020). The Zn-Cu binary system and ternary alloy systems obtained by adding different alloying elements to Zn-Cu binary systems have become an important area of study in recent years due to their high mechanical properties, elongation rates, and corrosion resistance (Liang et al., 2025; Morath et al., 2025; Liang et al., 2026; Yang et al., 2025).

Review of the Work Performed

In their study, Liang and his colleagues subjected pure Zn and Zn-0.4Cu alloys to ECAP processing at room temperature. Subsequently, they conducted testing procedures for microstructural examination, determination of mechanical properties, and identification of corrosion behaviour. While the grain size in pure Zn was 17.36 μm, after the ECAP process, the grain size in the Zn-0.4Cu alloy was found to be 2.15 μm. With the addition of copper, they determined that there were needle-like precipitates at the grain boundaries in the Zn-0.4Cu alloy, which were compatible with the matrix. They found that adding copper increased the tensile strength somewhat, but doubled the elongation. While the tensile strength (UTS) of pure Zn is 90 MPa, the tensile strength of the Zn-0.4Cu alloy is 130 MPa. Zn-Cu alloys, which have a fine-grained structure, showed better corrosion resistance compared to pure Zn. The corrosion rates of pure Zn and Zn-0.4Cu alloy were determined to be 270.72 μm/y and 186.34 μm/y, respectively. When they examined the types of corrosion, pure Zn exhibited more pitting corrosion, while grain boundary corrosion was observed in Zn-Cu alloys. Zn-Cu alloys have shown good compatibility with bone marrow stem cells in terms of biocompatibility. Liang et al. stated that the antibacterial and osteogenic properties of the Zn-Cu alloy yielded significantly better results compared to pure Zn, making these alloys a good candidate for biomedical applications (Liang et al., 2025).

Morath et al. investigated the biological effects of copper alloying in Zn-based biodegradable implants. They have worked on Zn-xCu (x: 0.8 wt% - 1.5 wt%) alloys. They examined the biocompatibility of these alloys with and without heat treatment. They determined that the Zn-1.5Cu alloy had the most biocompatible measurements compared to the Zn-0.8Cu alloy and pure Zn. Although the yield and tensile strengths are similar as a result of the tensile test, the mechanical properties of the heat-treated alloys are

superior. The yield strength, tensile strength, and elongation of the Zn-0.8Cu alloy after heat treatment are 112 MPa, 130 MPa, and 61%, respectively. The Zn-1.5Cu alloy has a yield strength, tensile strength, and elongation of 104 MPa, 125 MPa, and 76%, respectively. When researchers examined the corrosion rates, they found that the corrosion rates of the thermally treated Zn-0.8Cu and Zn-1.5Cu alloys after 10 days were 110 μm/y and 20 μm/y, respectively. Researchers have found that pitting corrosion occurs in all alloys. Overall, when evaluating the work of Morath and his colleagues, it is evident that the Zn-1.5Cu alloy exhibits similar mechanical and corrosion properties to other alloys, but demonstrates a more regular corrosion degradation compared to the others (Morath et al., 2025).

In their research, Liang and colleagues studied hot-rolled Zn-2.4Cu alloy. The results of tensile tests determined the yield strength, tensile strength, and elongation of the hot-rolled Zn-2.4Cu alloy to be 202.91 MPa, 230 MPa, and 4.60%, respectively. In their study, the researchers also examined the 60-day corrosion rate. They determined the corrosion rate to be 53 μm/year. They have shown that the resulting HT/Zn-2Cu alloy has strong antibacterial properties, minimizing biofilm degradation and bacterial growth. When they evaluated all the findings, they determined that it could be designed as a biodegradable material that simultaneously aims to heal bone tissue and reduce infection risks in clinical applications (Liang et al., 2026).

Yang et al. aimed to improve the mechanical properties of an alloy with 8 wt% Cu addition by applying hot rolling in this study, and to design a biodegradable Zn-Cu alloy with suitable biocompatibility. When they examined the microstructure of the Zn-Cu alloy, they observed the formation of a large-sized $CuZn_5$ phase. After hot rolling, they determined that the yield strength (YS), ultimate tensile strength (UTS), and elongation (EL) were 278.2

MPa, 330.8 MPa, and 25.46 %, respectively. When they examined the corrosion results, they found that the degradation rate of the binary Zn-8wt%Cu alloy was 104.9 μm/y, which is higher than that of pure Zn (71.9 μm/y). Adding 8 wt% Cu to pure Zn increased the corrosion rate of pure Zn. When researchers looked at their biocompatibility, they observed that the biocompatibility of the Zn-8wt%Cu alloy was good (Yang et al., 2025).

Result

When recent research is examined, it is observed that the mechanical properties of Zn-Cu alloys improve with an increase in the Cu ratio. Although corrosion rates varied with immersion time, the increase in Cu content generally showed a tendency to decrease the corrosion rate. Considering the requirements of biodegradable implant materials, it appears that a high copper content (wt% Cu > 2.5) yields better results. Zn-Cu alloys have gained attention in recent years as promising biodegradable materials due to their biocompatibility.

References

Hussain, M., Ullah, S., Raza, M. R., Abbas, N., & Ali, A. (2022). Recent developments in Zn-based biodegradable materials for biomedical applications. *Journal of Functional Biomaterials*, *14*(1), 1. https://doi.org/10.3390/jfb14010001.

Li, C., Guo, C., Fitzpatrick, V., Ibrahim, A., Zwierstra, M. J., Hanna, P., ... & Kaplan, D. L. (2020). Design of biodegradable, implantable devices towards clinical translation. *Nature Reviews Materials*, *5*(1), 61-81. https://doi.org/10.1038/ s41578-019-0150-z.

Liang, H., Wu, H., Yin, D., Yu, H., He, Z., Zhang, W., ... & Jiang, G. (2025). Potential of biodegradable Zn alloys with fine grains for orthopedic and antibacterial applications. *Materials Advances*, *6*(11), 3495-3511. DOI: 10.1039/D4MA01094A.

Liang, Y., Dai, J., Zhang, Z., Liu, A., Xu, J., Tang, H., ... & Li, Y. (2026). Osteogenic and antibacterial enhancement by alloying design and microstructural modification of additively manufactured biodegradable metals. *Biomaterials*, *324*, 123481. https://doi.org/10.1016/j.biomaterials.2025.123481.

Morath, L., Rahim, S. A., Baker, C., Anderson, D. E., Hinds, M. T., Sikora-Jasinska, M., ... & Goldman, J. (2025). The biological effects of copper alloying in Zn-based biodegradable arterial implants. *Biomaterials advances*, *167*, 214112. https://doi.org/10.1016/j.bioadv.2024.214112.

Qiao, W., Pan, D., Zheng, Y., Wu, S., Liu, X., Chen, Z., ... & Cao, X. (2022). Divalent metal cations stimulate skeleton interoception for new bone formation in mouse injury models. *Nature communications*, *13*(1), 535. https://doi.org/10.1038/s41467-022-28203-0.

Shuai, C., Dong, Z., He, C., Yang, W., Peng, S., Yang, Y., & Qi, F. (2020). A peritectic phase refines the microstructure and enhances Zn implants. *Journal of Materials Research and Technology*, *9*(3), 2623-2634. https://doi.org/10.1016/j.jmrt.2020.04.037.

Wu, C., Lin, F., Liu, H., Pelletier, M. H., Lloyd, M., Walsh, W. R., & Nie, J. F. (2025). Stronger and coarser-grained biodegradable zinc alloys. *Nature*, *638*(8051), 684-689. https://doi.org/10.1038/s41586-024-08415-8.

Yang, Y., Cui, D., Zhao, F., & Tan, Y. (2025). A strategy to simultaneously improve mechanical properties and biocompatibility of biodegradable Zn-Cu alloys as potential vascular stents. *Journal of Alloys and Compounds*, *1020*, 179468. https://doi.org/10.1016/j.jallcom.2025.179468.

BÖLÜM 5

A REVIEW OF HYDROXYAPATITE (HA) SURFACE COATINGS FOR BIODEGRADABLE IMPLANTS

1. HALİL EREN[1]

Introduction

The higher mechanical properties of metal alloys compared to ceramics and polymers make these materials more suitable for load-bearing applications. Bioinert materials are quite commonly used in the design of bone implants. Examples of these include stainless steel, titanium, and cobalt-chromium alloys (Chen et al., 2025; Vishnu et al., 2025). Although these alloys have quite good mechanical properties and biocompatibility, they pose some problems in terms of use due to their lack of biodegradability. After the bone tissue heals, the bioinert materials remain in the body. These materials can cause infection risks over time or lead to complaints arising from their presence in the patient's body (Chen et al., 2025; Taghipour et al., 2024). Secondary surgery is required to remove bioinert materials from the body. This situation carries serious negative consequences in terms of cost, psychological well-being,

[1] Lecturer Dr., Çankırı Karatekin University, Materials and Materials Processing Technologies Department, Orcid: 0000-0002-4224-683X

and health (Sousa et al., 2025). For these reasons, new-generation biodegradable alloys based on Mg, Fe, and Zn have been developed in recent years (Li et al., 2024).

In recent years, numerous studies have been conducted on magnesium and its alloys for various applications, including vascular stents and orthopedic implants (Zhang et al., 2025). However, the high corrosion rates of Mg alloys still significantly limit their applications (Hashemi et al., 2025). Due to the rapid degradation of magnesium, hydrogen release is quite high, which causes Mg alloys to lose their mechanical properties before bone tissue has healed (Ma et al., 2025; Ruggiero et al., 2025). Therefore, different methods have been applied to reduce the corrosion rate of magnesium alloys (Chen et al., 2025). Surface coating is one of these methods, and many studies have been conducted on it in recent years (Chen et al., 2025).

Iron (Fe) alloys are one of the most important types of biodegradable implant materials due to their high mechanical properties. However, corrosion rates are quite slow compared to Mg and Zn alloys. The integrity of mechanical strength and, especially for orthopedic applications, a balanced degradation rate are important (Wang et al., 2025). The main problem encountered in Fe alloys is that the very low corrosion rate leads to corrosion occurring over a longer period than the degradation time. In biodegradable applications, the key is to match the corrosion rate with the rate of tissue healing (Wang et al., 2025). Therefore, in recent years, researchers have turned their attention to studies aimed at increasing the corrosion rate of Fe alloys. Some surface treatments to be applied, along with alloying and processing, are among the methods to be developed to increase corrosion rates (Wang et al., 2025).

Although Mg alloys are an important biodegradable material due to their suitable biocompatibility and high mechanical properties, they pose a disadvantage due to their high corrosion rate.

Fe alloys, on the other hand, present a challenge because they exhibit very low corrosion rates. However, Zn alloys exhibit a degradation time that is compatible with the bone tissue repair process, making them a more ideal alloy in terms of corrosion (Wang et al., 2025). However, in some studies, the corrosion behaviour may need to be modified to strike a balance between bone growth and the fracture of metals. Therefore, the application of surface coating methods to maintain the corrosion rate in balance is seen as a new area for researchers (Li et al., 2024).

Hydroxyapatite (HA) is rich in phosphorus and calcium and is the most commonly used ceramic coating type in the human body. Bioceramics coatings are a method applied to the surfaces of biodegradable metals with the aim of improving the biocompatibility and corrosion resistance of the metals (Ren et al., 2025). It can accelerate the repair and formation of bone tissue in the human body, and is therefore frequently used in many implant products (Ren et al., 2025; Zhang et al., 2022). Studies have determined that HA coatings increase corrosion resistance. These coatings are being developed for application to many biodegradable orthopedic implant materials (Hernandez et al., 2022; Jiang et al., 2022).

Review of the Work Performed

In their study, Aksakal et al. investigated the corrosion changes and mechanical property effects of cold-rolled Zn-1Cu alloys by applying hydroxyapatite (HA). Before the coating process, SEM-EDS examinations revealed structures such as surface voids and capillary cracks. Researchers have found that these negative effects disappear after the coating process. Although coating processes have the characteristic of covering surface defects, the corrosion resistance before and after coating is similar (Aksakal et al., 2024). Researchers have attributed this to the low corrosion rates of existing Zn alloys. However, even though alloys exhibiting low

corrosion rates are still developed, their mechanical properties are also low. Controlling the rate of degradation, in particular, could serve as an inspiration for future studies. Researchers have stated that the study of Zn alloys is important, along with new coating techniques (Aksakal et al., 2024).

In another study, Aksakal et al. investigated the effect of HA coatings on the corrosion behaviour of Zn-1Cu-1Ag alloys. They determined that alloys with HA surface coatings have higher corrosion resistance (Aksakal et al., 2024).

In their study, Li et al. investigated the effects of hydroxyapatite coatings on magnesium alloys. Hydroxyapatite (HAP) coatings deposited on the surface have shown better corrosion resistance. In addition, their biocompatibility is also quite high (Li et al., 2024). Researchers have observed that these films, particularly ST-deposited composite films, exhibit quite good biodegradability due to the filiform nature of the surface types and the additional coating of HAP in a thick layer. In their current study, the researchers concluded that HAP/MgO composite coatings hold significant potential for biodegradable materials (Li et al., 2024).

In their study, Podgorbunsky et al. investigated magnesium and hydroxyapatite-based biodegradable composites for use in bone implants. As a result of their study, the researchers formed a PEO layer on the surface of the composite material, which improved the corrosion properties of the implant they aimed to develop (Podgorbunsky et al., 2025). The addition of HA nanoparticles to magnesium-based compounds increased their corrosion resistance in highly corrosive environments (Podgorbunsky et al., 2025).

In their study, Esmaeilnejad et al. created a calcium zinc phosphate coating on zinc alloys with HA/PLA to improve biocompatibility and corrosion behaviour. Researchers observed that

the coating layer applied resulted in a 26-fold and 12-fold reduction in the corrosion rate, respectively (Esmaeilnejad et al., 2025).

In their study, Shishir et al. worked on the development of biodegradable and corrosion-resistant hybrid coatings on Zn-1Mg alloys. Researchers have determined that the applied coatings increase the corrosion resistance of the Zn-1Mg alloy and exhibit biocompatibility (Shishir et al., 2024). In their current study, the researchers determined that the ceramic-polymer hybrid coating applied to the Zn alloy reduced the corrosion rate. In addition, they observed that their in-situ compatibility in a laboratory environment was quite remarkable. These situations indicate that the coating methods applied are ideal for the development of biodegradable implant materials (Shishir et al., 2024).

Result

Although Mg alloys, designed to be biodegradable, have a high corrosion rate, Fe alloys show a low corrosion rate, and Zn alloys exhibit degradation compatible with the bone healing process, researchers have worked on different corrosion improvement methods to balance corrosion rates. Among these, surface coating methods have been one of the methods focused on in recent years. HA coatings or composite/hybrid coatings obtained by combining HA have attracted considerable attention due to the fact that hydroxyapatites (HA) are rich in phosphorus and calcium and are the most commonly used type of ceramic coating in the human body. When examining the studies conducted, it is evident that surface coating methods are a highly successful method for balancing the corrosion rates of alloys. HA-based composite coating methods hold promise for the development of biodegradable materials for future studies.

References

Aksakal, B., Isın, E., Aslan, N., Cihangir, S., Sezek, S., & Yilmazer, Y. (2024). Influence of plastic deformation and hydroxyapatite coating on structure, mechanical, corrosion, antibacterial and cell viability properties of zinc based biodegradable alloys. *Metals and Materials International*, *30*(12), 3320-3337. https://doi.org/10.1007/s12540-024-01710-z.

Aksakal, B., Karadogan, S. A., Aslan, N., Fidan, F., Yilmazer, Y., & Sezek, S. (2024). The influence of cold rolling and hydroxyapatite coating on the mechanostructure, corrosion resistance, cell viability, and antibacterial activity of ZnCu biodegradable implants. *Journal of Materials Research*, *39*(11), 1701-1715. DOI:10.1557/s43578-024-01340-6
.

Chen, H., Wang, Y., He, L., Zhang, X., Mei, Y., Wu, T., ... & Tang, H. (2025). Surface engineering of biodegradable magnesium alloys as orthopedic implant materials: Recent developments and future prospects. *Coatings*, *15*(2), 191. https://doi.org/10.3390/coatings15020191.

Esmaeilnejad, A., & Yarmand, B. (2025). Improving biocompatibility and corrosion behavior of biodegradable zinc implant using a calcium zinc phosphate layer sealed by hydroxyapatite/polylactic acid. *Surface and Coatings Technology*, 132760. https://doi.org/10.1016/j.surfcoat.2025.132760.

Hashemi, T. S., Jaiswal, S., Celikin, M., Mccarthy, H. O., Levingstone, T. J., & Dunne, N. J. (2025). Strategically designed bioactive dual-layer coating of octacalcium phosphate and dicalcium phosphate dihydrate for enhancement of the corrosion resistance of pure magnesium for orthopaedic applications. *Surface and Coatings*

Technology, *495*, 131556. https://doi.org/10.1016/j.surfcoat.2024.131556.

Hernandez, L., González, J. E., Barranco, V., Veranes-Pantoja, Y., Galván, J. C., & Gattorno, G. R. (2022). Biomimetic hydroxyapatite (HAp) coatings on pure Mg and their physiological corrosion behavior. *Ceramics International*, *48*(1), 1208-1222. https://doi.org/10.1016/j.ceramint.2021.09.206.

Jiang, D., Li, Q. K., Liu, Y. Z., Xiao, Z., Xia, B. H., Li, S. Q., ... & Zeng, R. C. (2022). Polyphosphate assisted hydrothermal synthesis of hydroxyapatite coating on Mg alloys: enhanced mechanical properties and corrosion resistance. *Surface and Coatings Technology*, *432*, 128033. https://doi.org/10.1016/j.surfcoat.2021.128033.

Li, X., Lin, E., Wang, K., Ke, R., Kure-Chu, S. Z., & Xiao, X. (2024). Fabrication and characterization of hydroxyapatite coatings on anodized magnesium alloys by electrochemical and chemical methods intended for biodegradable implants. *Ceramics International*, *50*(19), 36838-36848. https://doi.org/10.1016/j.ceramint.2024.07.071.

Ma, S., Zhang, D., Zhang, P., & Markert, B. (2025). Rapid prediction of the corrosion behaviour of coated biodegradable magnesium alloys using phase field simulation and machine learning. *Computational Materials Science*, *247*, 113546. https://doi.org/10.1016/j.commatsci.2024.113546.

Podgorbunsky, A. B., Imshinetskiy, I. M., Mashtalyar, D. V., Sidorova, M. V., Gnedenkov, A. S., Sinebryukhov, S. L., & Gnedenkov, S. V. (2025). Bioresorbable composites based on magnesium and hydroxyapatite for use in bone tissue engineering: Focus on controlling and minimizing corrosion activity. *Ceramics*

International, *51*(1), 423-436. https://doi.org/10.1016/j.ceramint.2024.11.016.

Ren, J., Zhao, Z., Li, H., Wang, D., Shuai, C., & Yang, Y. (2025). Surface coatings on biomedical magnesium alloys. *Materials*, *18*(14), 3411. https://doi.org/10.3390/ma18143411.

Ruggiero, R., Marano, R. M., Marrelli, B., Facente, A., Aiello, E., Conte, R., ... & Tatullo, M. (2025). Enhancing magnesium-based materials for biomedical applications using an innovative strategy of combined single point incremental forming and bioactive coating. *Journal of the Mechanical Behavior of Biomedical Materials*, *163*, 106858. https://doi.org/10.1016/j.jmbbm.2024.106858.

Shishir, R., Nasiruddin, U., Ponnilavan, V., Rama Krishna, L., & Rameshbabu, N. (2024). Development of corrosion-resistant and bioactive ceramic-polymer hybrid coating over Zn-1Mg biodegradable implant material. *Surface and Coatings Technology*, *487*, 131031. https://doi.org/10.1016/j.surfcoat.2024.131031.

Sousa, A. M., Branco, R., Morais, P. V., Pereira, M. F., Amaro, A. M., & Piedade, A. P. (2025). Evaluation of the interface of metallic-coated biodegradable polymeric stents with prokaryotic and eukaryotic cells. *Bioactive Materials*, *46*, 55-81. https://doi.org/10.1016/j.bioactmat.2024.12.003.

Taghipour, S., Vakili-Tahami, F., & Chakherlou, T. N. (2024). Comparing the performance of a femoral shaft fracture fixation using implants with biodegradable and non-biodegradable materials. *Biomedical Physics & Engineering Express*, *11*(1), 015014. DOI 10.1088/2057-1976/ad90e7.

Vishnu, J., Praveenkumar, K., Kumar, A. A., Nair, A., Arjun, R., Pillai, V. G., ... & Shankar, K. V. (2025). Multifunctional zinc oxide loaded stearic acid surfaces on biodegradable magnesium WE43 alloy with hydrophobic, self-cleaning and biocompatible attributes. *Applied Surface Science*, *680*, 161455. https://doi.org/10.1016/j.apsusc.2024.161455.

Wang, A., Zhao, M., Ji, J., Sun, Y., & Liu, W. (2025, February). State of art on enhancing the corrosion rate of biodegradable iron alloys. In *Journal of Physics: Conference Series* (Vol. 2959, No. 1, p. 012012). IOP Publishing. DOI 10.1088/1742-6596/2959/1/012012.

Zhang, A. M., Lenin, P., Zeng, R. C., & Kannan, M. B. (2022). Advances in hydroxyapatite coatings on biodegradable magnesium and its alloys. *Journal of Magnesium and Alloys*, *10*(5), 1154-1170. https://doi.org/10.1016/j.jma.2022.01.001.

Zhang, A., Fan, X., Yang, Z., Xie, Y., Wu, T., Zhang, M., ... & Chen, W. (2025). Optimized design and biomechanical evaluation of biodegradable magnesium alloy vascular stents. *Acta Mechanica Sinica*, *41*(3), 624055. https://doi.org/10.1007/s10409-024-24055-x.

GEÇİCİ KAPAK

Kapak tasarımı
devam ediyor.